AZƏRBAYCAN MİLLİ ELMLƏR AKADEMİYASI

AZƏRBAYCAN ASTRONOMİYA JURNALI

2018, Cild 13, № 1

AZERBAIJAN NATIONAL ACADEMY OF SCIENCES

ASTRONOMICAL JOURNAL OF AZERBAIJAN

2018, Vol. 13, № 1

Bakı-2018 / Baku-2018

ASTRONOMICAL JOURNAL OF AZERBAIJAN

Founded in 2006 by the Azerbaijan National Academy of Sciences (ANAS)
Published in the Shamakhy Astrophysical Observatory (ShAO) named after N. Tusi, ANAS
ISSN: 2078-4163 (Print), 2078-4171 (Online)

Editorial board

Editorial Office address:	ANAS, 30, Istiglaliyyat Street, Baku, AZ-1001, the Republic of Azerbaijan
Address for letters:	ShAO, P.O.Box №153, Central Post Office, Baku, AZ-1000, Azerbaijan
E-mail:	aaj@shao.az
Phone:	(+994 12) 510 82 91
Fax:	(+994 12) 497 52 68
Online version:	http://www.aaj.shao.az

ASTRONOMICAL JOURNAL OF AZERBAIJAN

2018, Vol. 13, № 1

Contents

EFFECT OF SOLAR ACTIVE PHENOMENA ON THE ENVIRONMENT SPACE AND ITS FORECAST

V. N. Ishkov*

Pushkov Institute of Terrestrial Magnetism, Ionosphere and Radio Wave Propagation, RAS

Investigations of active phenomena on the Sun in recent decades leave no doubt that the state and all significant short-term disturbations of environment space are determined exclusively by solar flare events and regions in the corona of the Sun with a magnetic field open to interplanetary space (coronal holes). The interaction of new emerging magnetic fluxes with already existing magnetic fields leads to the occurrence of solar flares (in active regions) and solar filament ejections (outside of them). Observation of the emergence of new magnetic fluxes, assessment of their magnitude and the rate of ascent allow us to predict solar flares and filament ejections and to estimate the degree of their geo-effectiveness. The main agent that visualizes the propagation of disturbances from solar flares and filaments in the corona of the Sun and in interplanetary space is the coronal mass ejections whose characteristics ideally allow one to estimate the possible disturbances of the geomagnetic field, the possible growth of charged particle fluxes of high energies in environment space. For successful forecasting of geo-effective active phenomena on the Sun and their consequences in environment space. It is necessary to know the situation on the Sun for the last 3 days, taking into account the development and characteristics of the current cycle and the epoch of solar activity.
PACS: code

Keywords: Active solar phenomena – Space weather – Forecast of solar activity – Forecast of environment space

1. INTRODUCTION

The beginning of the space age has become a new step in the exploration of the Earth in a broad sense, from its depths to the boundaries with the heliosphere, both ground-based instruments and those installed on board spacecraft. The ever-increasing rates of space exploration put the problem of assessing and

* E-mail: ishkov@izmiran.ru

forecasting solar activity (SA) in all its manifestations, as well as the state of the space environment, both near the Earth (space weather) and in any given region of the heliosphere.

In this paper, environment space is understood as the region starting from a height of 50-60 km above the Earth and extending for a distance of tens of terrestrial radii to the boundaries with the heliosphere, in which its filling substance is still more connected with our planet, and not with the Sun or some other astronomical body. It is clear that in this area we deal mainly with natural plasma. The term "SPACE WEATHER" now refers to the state of the upper layers of the Earth's atmosphere (mesosphere, thermosphere), magnetosphere, and ionosphere - all layers of environment space. at any given time.

Currently, there has been a complete understanding that the Sun itself and the active phenomena in its atmosphere have a major effect on environment space.

2. PHYSICAL AND OBSERVATIONAL PRINCIPLES OF SOLAR ACTIVITY FORECAST

Solar activity is usually called the entire set of observed phenomena in the solar atmosphere, causing changes in its radiation in different ranges of electromagnetic waves and fluxes of particles of different energies. These changes in the optical range are manifested in a change in the number of different solar structures and are not almost noticeable in the optical radiation range; the change in the solar constant is $\leq 0.1\%$. However, in soft X-ray radiation, these changes are manifested in the number of structures and in radiation: the difference between the level of "background" radiation in the range 1-8Å (1-12.5 Kev) at the maximum and at the minimum of the SA exceeds two orders of magnitude (more than 100 times). The state of CA is characterized by observational indices, the longest series has a relative number of sunspots (W). This index was first introduced by R. Wolff, and it has been determined since 1849 (reliable series W1), when regular observations of sunspots began to lead several observatories in Europe. In addition, Wolf restored the monthly averages of this index to 1749 (numbered series W2) and the average annual to 1700, according to fragmentary data of individual European observers. Modern researchers on the published data qualitatively extended this series until 1610 (Fig. 1). Almost all researchers used in their works the series of W2, and many not taking into account their reliability. Therefore, in [1] the series W1 and W2 were compared and their consistency was verified. The analysis showed that for time intervals (1749-2016) and (1849-2016) significant differences in the position and value of the fundamental harmonic and its spectral width were revealed. In addition, comparison of the series implies a distinctive character of the behavior of the main characteristics of the series in the interval

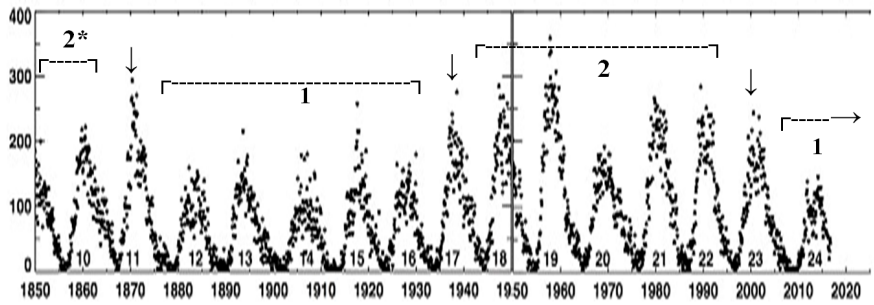

Fig. 1. Reliable series (W1) of the relative sunspot numbers with the boundaries of the structural epochs of lowered (1) and increased (2) SA with transitional cycles between them; 2* - probable period of increased solar activity, including solar cycles 10 - 6. The figure is converted from https://history.aip.org/climate/solar.htm

from 1749 to 1849, and an increase in the length of this series leads to a deterioration in the resolution of some important spectral characteristics (usually vice versa) and a significant distortion of the "high-frequency" part of the spectrum of the reconstructed series. All this raises the question of the correctness of using the restored part of the series in most applications. In other words, to study the effect of SA on various long-term processes, it is possible to use only a reliable series of Wolf numbers (1849 - 2016) from the middle of the 9th and 24th cycles of the SA. At the same time, as shown in [2], it is possible to conditionally include SCs 8 and 9 in the statistics of reliable solar cycles (SC), which adjoin to reliable and non-contradictory characteristics of a reliable series of SCs, thereby increasing statistics for up to 17 SA cycles.

A reliable series of Wolf numbers shows an amazing consistency in the main manifestations of the development of individual 11- and 22-year-old SCs and the structure of its cyclicality implies a periodic change of epochs "elevated" (SC 6,7,7,8,10,18-22) and "low" 12 - 16, 24 - and 4 subsequent) SA, each for five cycles [3]. The principal differences in the characteristics and basic properties of SCs of different epochs of SA are determined by a different range of changes in the values of the mean values of the total magnetic field of the sun, which is manifested in the nature of the stain-forming activity, and hence in active phenomena on the Sun and in the characteristics of the interplanetary magnetic field. Between these epochs transitional periods are observed (SC 11, 23 and 17), during which the nature of the stain-forming activity changes in about 15 years. The regimes of generation of magnetic fields in the spot-forming zone of the Sun, which leads to changes in the general magnetic field of the Sun. In the summary Table 1 the basic numerical parameters of reliable SC of the corresponding epochs and transitional periods are given.It should be noted that within the epochs of SA all

observational rules for the development of the SA are fulfilled, such as the rule of GNEVYSHEV-OHL, according to which every even cycle is lower than the subsequent odd one. In transition periods, these rules can be infringed which happened in SC 22 and 23, which were quite unusual in their characteristics and, to some extent, violated the current picture of the development of SC [4].These features are completely explained by the transition period from the era of increased to epoch of lowered SA [3]. The current 24 SC develops as a cycle of low magnitude, whose flare activity is substantially lower than all previous SCs of the space age, and opens the second epoch of the lowered SA. Based on the observational characteristics of this epoch (Table 1) and the stability of the solar cyclicity scenario, one can confidently predict that the next 4 SCs will be medium and low cycles.

Solar studies of recent decades have left no doubt that extremely large flare events and coronal holes (CHs) are completely determining the state of the environment space by geo-effective phenomena on the Sun. We classify the class of flare phenomena as:

- Solar flares with the entire spectrum of dynamic manifestations of the motion of matter and radiation in all ranges of the electromagnetic spectrum,

- Solar filament ejections with all their attendant phenomena.

Solar flares occur in active regions (AR) with groups of sunspots or without them or represent the reaction of the solar atmosphere to a fast process of energy release, which leads to a sharp local heating of all layers of the solar atmosphere, the appearance of various types of dynamic phenomena accompanied by the generation of powerful electromagnetic radiation in a wide range of frequencies from γ-quanta to kilometer radio waves and electron particle fluxes, protons, neutrons and heavy nuclei.

Solar filaments are clouds dense and cooler than the surrounding medium, plasma, which in the magnetic field of the solar atmosphere acquire the form of long formations elongated along the line of separation of polarities. The majority of filament or filament channels (the initial and, possibly, the final stage of the evolution of filament) select a neutral line along the entire surface of the Sun. Since the ARs are always bipolar structures, they are either formed in the regions on either side of the neutral line, or their formation entails a rearrangement of the large-scale magnetic field, and the polarization line still appears inside the AR.

Accordingly, the filaments are almost always present in all ARs, when directly in the form of a filaments, when in the form of a filaments channel, depending on the complexity and magnitude of the magnetic field of the AR. Ejections of solar filaments in the vast majority of cases occur outside the AR in small magnetic fields ($<$50 Gs') and with observations with a good resolution, starting with the accelerating rise of the entire body of the filaments or a part of it, two emission ribbons of reduced brightness rapidly form, stretching along the polarity, previ-

Table 1. Solar cycles of reliable increased and lowered epochs and periods of solar activity reorganization. T_0 is the commencement of SC; W*m is the initial value of smoothed Wolf numbers; TM is time of the SC maximum; WM* is the maximum value of smoothed Wolf numbers; TY↑ is the duration of growth branch in terms of years; TY↓ is the duration of decay branch in terms of years; TY is the SC duration in terms of years; T_{1m} and T_{2m} are the duration of the minimum phase before and after this SC in terms of months; Spless are the number of spotless days in the corresponding minimum phases; and $\sum$ are average values over epochs. Reference solar cycles of transition periods are shown in bold

N	T_0	W^*_m	T_M	T_e	W^*_M	$T_Y\uparrow$	$T_Y\downarrow$	T_Y	$T1_m$	$T2_m$	S_pless
1.1. Solar cycles of a reliable epoch of increased SA											
18	1944 II	7.7	1947 V	1954 III	151.8	3.2	7.0	10.2	33^m	33^m	444
19	1954 IV	3.4	1958 III	1964 IX	201.3	3.9	6.5	10.4	33^m	38^m	221
20	1964 X	9.6	1968 XI	1976 VI	110.6	4.1	7.8	11.8	38^m	69^m	269
21	1976 VI	12.2	1979 XII	1986VIII	164.5	3.5	6.8	10.2	69^m	33^m	273
22	1986 IX	12.3	1989 VII	1996 V	158.1	2.9	6.7	9.6	33^m	40^m	308
Σ		9.2			157.26	3.52	6.96	10.44	41.2^m		302
1.2. Solar cycles of a certain epochs of lowered SA											
12	1878XII	2.2	1883XII	1890II	74.6	5.0	6.3	11.3	65^m	59^m	732
13	1890III	5.0	1894I	1901II	87.9	4.5	8.2	12.1	59^m	77^m	937
14	1902 I	2.6	1906II	1913VII	64.2	4.1	7.6	11.7	77^m	59^m	1045
15	1913VIII	1.5	1917VIII	1923VII	105.4	4.0	6.1	10.1	59^m	48^m	526
167	1923VIII	5.6	1928IV	1933VIII	78.1	4.7	5.6	10.3	48^m	54^m	666
Σ		3.4			82.44	4.5	6.5	10.9	61^m		781
24	2009 I	1.7	2014IV	2020V-IX	81.9	5.25	5.9	12	68^m	59^m	
1.3. Solar cycles of reliable periods of SA reorganization											
10	1855XII	3.2	1860 II	1867 II	97.9	4.17	7.25	11.42	38^m	34^m	402
11	1867III	5.2	1870VIII	1878 XI	140.5	3.42	8.50	11.92	34^m	65^m	1025
16	1923VIII	5.6	1928 IV	1933VIII	78.1	4.7	5.6	10.3	48^m	54^m	666
17	1933IX	3.4	1937 IV	1944 I	119.2	3.6	6.9	10.5	54^m	33^m	262
22	1986IX	12.3	1989 VII	1996 V	158.1	2.9	6.7	9.6	33^m	40^m	308
23	1996VI	8.0	2000 IV	2008 XII	120.7	3.8	8.9	12.7	40^m	68^m	821

ously denoted by a filament, in which flare arched structures become visible in tens of minutes - a typical picture of a two-ribbon flare, i.e. emissions of filaments

outside the AR can be represented as flares with a slow increase in intensity to a maximum ($>$ 1 hour) and a significant decrease in intensity ($>$ 3 hours). In AR, large flares are often accompanied by the ejection of filament that either precede the flare itself (rarely), or, if there is a complete series of observations of the flare process, the filaments is ejected during the explosive phase of the flare.

Flare phenomena, as shown in [5], are a consequence of the interaction of new emerging magnetic fluxes (EMF) with already existing magnetic fields, both in AR and outside them. The most successful attempt to classify the phenomenon of EMF with respect to flare activity first made in the work of Golovko [6,7]. Depending on the magnitude and lifetime of the magnetic flux, three evolutionary branches of the population of the EMF on the Sun were identified, and among them, which is very important, the EMF with rapid evolution were identified. These studies allow us to consider the process of implementing large solar flares as an independent process within the overall development of the AR, which produces a environment space with rapid evolution. Limited in time, such a process of emergence of a new magnetic flux can accelerate the evolution of the AR, but, in general, such an influence can be considered insignificant, since AR continues to exist due to internal evolutionary changes associated with the parent magnetic flux.

In the general case, the AR phenomenon itself should be considered as the appearance and development of one or several close EMFs ($\sim 10_{13}$ Wb), simultaneously or successively emerging into the solar atmosphere with a low (evolutionary) rate of ascent ($1.7 \cdot 10_{12}$ Wb / day by estimation [7]), which develops from the appearance of the first signs of the floccula, through the stage of formation, development and decay of the sunspot group until the floccula completely disappears.All phases of AR development can occur the emergence of new magnetic fluxes whose magnetic field interacting with the magnetic field of the AR, always causes an increase in flare activity proportional to the amount of energy that has been supplied with the new EMF, which opens a new direction in approaches to forecasting large solar flares [5].

From the observations of the EMF, one can summarize the signs, after which increase in flare activity is observed:

- For large solar flares, it is necessary that the new FMF be large enough ($>$ 10_{13} Wb) and the speed of its ascent should be at least $5 \cdot 10_{12}$ Wb / day;

- large solar flares appear 1 to 2 days after the detection of EMF within the AR, which is true for the epoch of increased SA and transition period SC 23, when these studies were carried out, however, in 24 SC, in the epoch of lowered SA, this time interval was only 1 ± 0.5 days [3];

- Flares of large and medium class in the AR are grouped together in a series, processions [5, 8], which occur in a limited time interval and, importantly, are

genetically related to one EMF.

The interval of time for which the main share of flares of large and medium class is carried out in the AR is the period of flare energy release. Depending on the degree of development of the AR, the characteristics of its magnetic field, the magnitude, structure and rate of ascent of the new EMF, this period may take on average 55±30 hours or 16% of time of the AR passage along the visible disk of the Sun, [5]. The rapid growth of the area of the sunspot groups, their number, the rapid complication of the magnetic and spatial structure of the AR, a significant increase in the background values of the fluxes of soft X-ray radiation and radio flux are the main signs of the emergence of a new EMF. These signs allow us to forecast the period of flare energy release in a day or two before the realization of large solar flares.

The coronal holes are extended regions in the corona of the Sun with reduced density and temperature, characterized by a radiation deficit in some spectral lines of the extreme UV, X-ray and microwave ranges with a magnetic field that is open to interplanetary space. A large CH usually has 3 to 8 solar rotations, practically without changing its position. However, its visible boundaries can be shifted to 20°/day, changing its dimensions or shifting it as a whole [9]. Geo-effective are CHs in the range of heliosphere N30° – S30°, the extent of $\geq 10°$ in heliosphere, the area ≥ 5000 thousandths of the visible hemisphere [10], and localized in enhanced background magnetic fields. The solar plasma is not supported by magnetic forces and easily enters the interplanetary space, creating high-speed streams of the solar wind with typical velocities of 500-700 km $s^{-}1$ with increased interplanetary magnetic field, density and temperature.

When passing through such a high-speed stream, the Earth's magnetosphere interacts with it, responding to geomagnetic disturbance. CHs are the most long-lived geo-effective phenomena on the Sun are sources of recurrent magnetic storms. Particular attention should be paid to the role of CH as amplifiers of geo-effectiveness of solar flare phenomena. The presence of a coronal hole near the AR or the location of the solar filament ejections sharply increases their geo-effectiveness, and expands the range of their localization. An example is the event on 14.04.1994, when the release of a high-latitude ($S50°$) filament located under a large CH led to a complete rearrangement of the magnetic structures of the southern hemisphere of the Sun and to a large magnetic storm of 17.IV.1994 [11].

3. THE EFFECT OF SOLAR ACTIVE PHENOMENA ON THE ENVIRONMENT SPACE (SPACE WEATHER)

Electromagnetic influences from flare events appear almost at the moment of the development of the process, while corpuscular and plasma disturbances

through the solar wind, propagating in the heliosphere, affect the magnetospheres of planets, their satellites and comets, causing significant deviations from the background, and quite state in almost all layers of their atmospheres.

The agents transmitting these disturbances from the Sun through the heliosphere and directly affecting the environment space are:

- Coronal mass ejection (CME), which are the result of active explosive and evolutionary processes in flares and filament ejections; observations and characteristics of CME make it possible to determine the direction of motion of the disturbances in the interplanetary space and to assess the possibility of its arrival in the CH;

- high-speed streams of solar plasma following the shock wave from large flare events or expiring from areas with an open magnetic field configuration - CH.

Disturbances from a large flare event can represented in three stages of impact [http://swpc.noaa.gov/NOAAscales], which are realised consistently in the environment space. First, at the time of the development of a geo-effective solar flare, the environment space is irradiated with a flux of electromagnetic radiation (R-electromagnetic shock). Then, after a time interval of a few minutes to 10 hours depending on the energy, the environment space receives the streams of solar charged particles (S is the corpuscular impact - the solar proton event), and finally, after 17-96 hours, density and temperature (G - plasma shock), causing disturbances in the geomagnetic field - magnetic storms. Note that the solar filament ejections and CHs cause only magnetic disturbances in CH.

According to this classification, a five-point scale for assessing the intensity of each of the impacts and their number in the environment space is introduced. It should be noted that this disturbance scale in the environment space was introduced in end of the last century and, accordingly, took into account the number of events of each class of disturbance only for the epoch of increased SA, i.e. for solar cycles of 20 - 22. Over the years, it became clear that the 23 cycle was transitional between the epochs of increased and lowered SA, and 24 cycle was the first solar cycle of the latter.

Therefore, we introduced observational data on the number of events for the respective epochs using the new data: for the transitional period of 23 SC preliminary results of studies of solar and geomagnetic disturbances in SC 17 (transitional between epochs of increased and lowered SA), and for the epoch of lowered SA by SC 24 –the preliminary results of studies of geomagnetic disturbances of the first epoch SA (SC 12-16), according to the data of the geomagnetic Aa-index and observations of the arrival of interplanetary shock waves from the recording of sudden impulses of the geomagnetic field SI and the sudden onset of magnetic storms (SSC), according to observations of the network that was already operating at that time geomagnetic stations [12].

Electromagnetic shock (R) - occurs at the time of the development of the solar flare, during which in the short-wave ranges of electromagnetic radiation the flux rises by several orders of magnitude relative to the background values. For example, in the soft X-ray band 1-8 Å (12.5-1 keV), the increase in the flux can reach four orders of magnitude. As a result of this action, sudden ionospheric disturbance develop in the ionosphere immediately at the time of the flare development (the characteristic time of onset of the disturbance development - minutes after the onset of the flare), causing a complete radio silence in the high-frequency band on the illuminated side of the Earth, which lasts for several hours, disrupting the radio communication on the illuminated side planet Fig. 2. In the low-frequency range, errors in GPS navigation systems for determining the positions of terrestrial objects and satellites increase and accumulate over many hours. The number of events varies from R1 for X-ray flares of M1 class (up to 2000 events per cycle in the epoch of increased SA and up to 800 - in the epoch of lowered), to R5 for the most powerful flares, whose X-ray score is $\geq$17.5 ($\sim$ 1 - 2 events for the solar cycle in the epoch of the increased SA, there is a high probability there are no events in the era of the lowered and $\geq$ 3 events in the transition period).

Corpuscular shock - the arrival in the environment space of solar high-energy

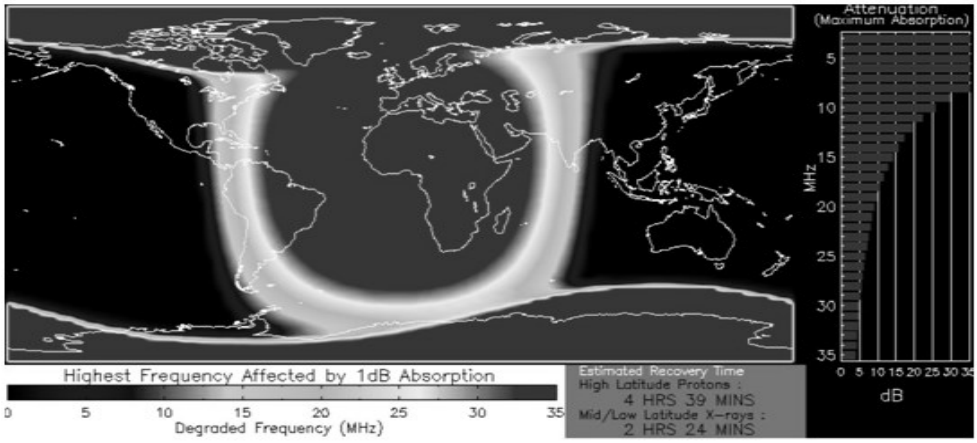

Fig. 2. Practically complete radio silence (oval) in the range 10-30 MHz during a large solar flare X9.3 / 2B on September 6, 2017 due to a sudden ionospheric disturbance (http//:www.spaceweather.com)

particles (protons, electrons, neutrons), which cause solar proton events (SPE). The invasions of high-energy solar particles (Epr$>$ 10 MeV) Fig. 3 significantly increase the level of radiation hazard for astronauts, crews and passengers of high-altitude aircraft at high latitudes, lead to satellite losses and the failure of scientific and navigation equipment on space objects, interrupt the implementa-

tion of short-wave communication in the circumpolar regions and contribute to a sharp increase in errors in navigation systems. This leads to serious difficulties in determining the coordinates of terrestrial and cosmic objects. The characteristic time for the onset of SPE relative to the beginning of a proton flare is a clock, although particles with GeV energies arrive to Earth a few minutes after the injection time in flares. The number of events varies for S1 to $\sim$ 50 - 40 events per cycle, and for S4 $\sim$ one for the increased SA epoch and up to five in the transitional period for the solar cycle.

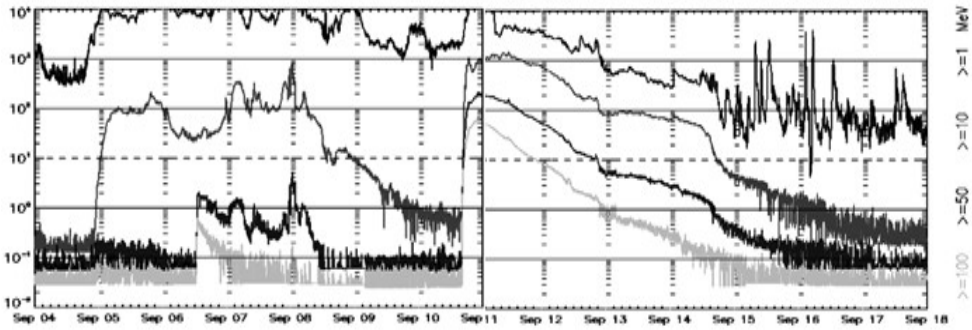

Fig. 3. The flux of solar high-energy protons in September 2017, from large solar flares in one active region according to the geostationary space observatory GOES-11 (Http//:www. swpc.noaa.gov).

Plasma shock - interplanetary shock waves and the subsequent fluxes of solar plasma of increased density and velocity (interplanetary ejections of the CME, high-speed solar wind streams) cause magnetic and ionospheric disturbances in the environment space. The disturbances of the geomagnetic field of the Earth (Fig. 4), whose intensity exceeds the threshold of magnetic storms, G1, in which at least one three-hour Kp-index has reached a value of 5, there are at least 1700 events for the solar cycle of the increased and 700 lowered, and events of intensity G5 (Kp = 9) are observed on the average 1 to 5 times for the solar cycle of any epoch. It should be borne in mind that this class estimates the intensity of the geomagnetic disturbance - it is entirely possible to imagine a situation where the geomagnetic disturbance has a class of G1 or G2, but there is actually no magnetic storm and the average daily geomagnetic Ap-index will be much smaller than the threshold of the magnetic storm. In this case, we are talking about a geomagnetic substorm. Of course, this is a matter of defining the concept of "magnetic storm" - a magnetic disturbance lasting not less than 12 hours and an average Ap-index of the disturbances reaches a value of 27 (in the western countries, the threshold value is Ap = 30).

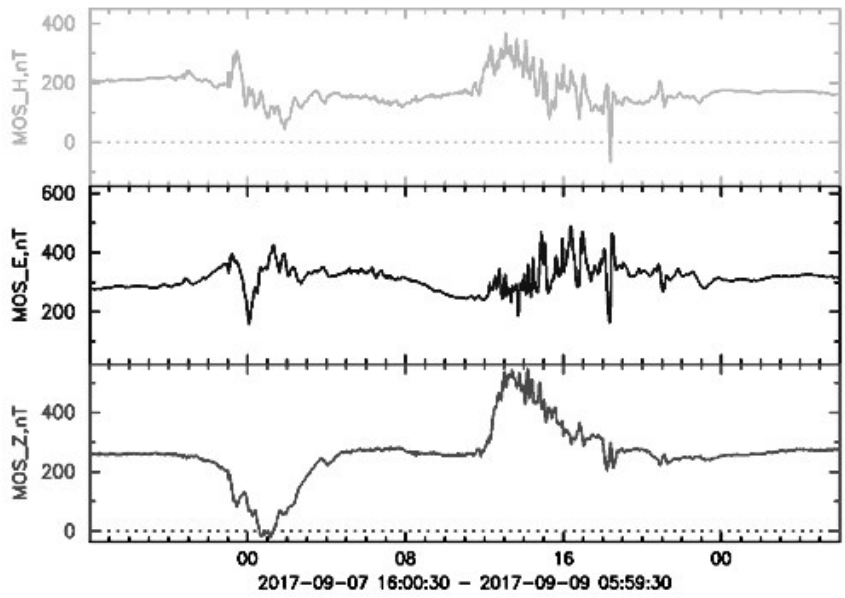

Fig. 4. Very strong magnetic storm (G4) 7 - September 8, 2017 according to the data of the geomagnetic observatory IZMIRAN. A record is given of the three components of the Earth's magnetic field.

At present, the problem of reflecting the situation in the environment space and assessing its status is being decided by the services of "SPACE WEATHER", which are created at leading institutes and organizations around the world (more than 40 addresses), the main of which are: in the USA (NOAA SWPC - http://www.swpc.noaa.gov), in Europe (ESA - http://www.esa-spaceweather.net/spweather/current_sw/index.html), WDC for CA indexes in Brussels - http://sidc.oma.be/html/LatestSWData.html#SUN), in Japan (http://hiraiso.nict.go.jp), in Australia (http://www.ips.gov.au/); in Russia: IZMIRAN (http://www.izmiran.ru/services/saf/), SRI RAS (http://www.iki.rssi.ru/sw.htm), IPG (http://ipg.geospace.ru/center-of-geliogeophysics/). Their task is to give in real time the main characteristics of phenomena that determine the state of environment space and indices characterizing the state of the magnetosphere, ionosphere and other layers of the earth's atmosphere. The most informative pages of data on the state of space weather are provided to us by the Sun Service Center of the Laboratory of the State of environment space the National Laboratory for Environmental Research (SWPC NOAA USA) - http://www.swpc.noaa.gov.

4. FORECAST OF GEO-EFFECTIVE SOLAR PHENOMENA AND THE STATE OF ENVIRONMENT SPACE.

Under the forecast of geo-effective solar phenomena, here we mean a set of all types of forecasts; whose task is to calculate the development of processes and phenomena occurring in the solar atmosphere and directly affect the magnetic and radiation environment in the environment space for specified time intervals, taking into account the characteristics of the current epoch of the SA. The time intervals for which a forecast is possible are determined by the characteristics of the physical processes of the emergence of new magnetic fluxes in the solar atmosphere, the nature of their interaction with the existing magnetic field, and the patterns laws of the appearance and evolution of solar structures, such as solar flare events and CHs.

Understanding the observational principles of the implementation of the scenario of solar cyclicity and the interaction of new EMF with existing magnetic fields led in 1990 to the creation in IZMIRAN of the methodology of short-term forecasts of solar active phenomena and their consequences in all three classes of disturbances in the environment space [13]. Weekly review of the state of SA and the environment space is published on Mondays on the pages of IZMIRAN: Russian version http://www.izmiran.ru/services/saf/, and English http://www.izmiran.ru/services/saf/?LANG=en. Each first Monday of the month is additionally given an overview of the development of the current SC and the preliminary values of the main indices of solar and geomagnetic activity.

By the time of arrival of disturbances to the Earth, it can be argued that the daily forecast of the state of environment space can be the most informative, but in real life such only specialized forecast groups can provide a forecast duty group. For scientific support of the forecast data, we can agree with a 3-day interval, which provides complete information on recurrent disturbances, but a "dead zone" for sporadic disturbances already appears. In our forecast, we selected a weekly forecast interval with additional releases when there are signs or a geo-efficient flare event that works well in the phases of growth, decline and minimum of SC, however, in the conditions of flare activity of several ARs simultaneously, serious difficulties arise. Therefore, if there is a need to support a project and with the rapid variability of the state of the environment space, a daily forecast is provided to the consumer. When making the forecast:

- All significant ARs are taken into account and, in case of appearance of the first signs of new EMF, estimation of the rate of ascent and, as developing; their magnitude is estimated;
- All significant, possibly geo-effective, solar flares are recorded;
- The solar filaments in which there are signs of instability are identified;

- The characteristics of all CME associated with observed flare events are analyzed;
- All CHs in the zone of influence on the Earth are evaluated from the point of view of their geo-effectiveness.

The structure of the review has remained unchanged all this time and includes a title and several sections, the first paragraph of the section being the actual review, and the second, the forecast for the next week:

- **The header** in which the time periods of the highlight and forecast, the number and commencement of the Carrington rotation of the Sun are indicated which makes it possible to determine the absolute longitudes of the solar structures, the position of the Earth relative to the ecliptic, and the heliospheric zone of geo-effectiveness of active phenomena for a given period;
- **The section of the state** of sunspot activity of the Sun with a 4-level evaluation of spot-forming activity (very low - W$\leq$11, low-W$\leq$30, medium-W$\leq$80, high-W$>$ 81), with a calculated mean value of the relative number of sunspots for the past week and the number of sunspot group sunspots on the visible disk of the Sun; for all large or flare-active sunspot group, their evolutionary and flare characteristics are given; in the next paragraph the forecast of spot-forming activity for the following week is given;
- **The state of the flare activity** gives its level (very low - flares of X-ray class B, low - C, medium - M1 - M4.9, high - M $\geq$ 5), the number of solar filament ejections and the number of CME (class, angular width); the table of the main characteristics of solar flares of an X-ray class $\geq$ M1 and all recorded solar filament ejections indicating the dynamic phenomena associated with them and a forecast of the level of flare activity for the next week;
- **The table** of CHs observed on the visible disk of the Sun with their coordinates, the area in Mm2, the age in solar rotations and the geo-effectiveness on the previous rotation;
- The section of information on the **sectoral boundaries** of the interplanetary magnetic field, the sector sign and the forecast of the date of the next sectoral boundary;
- **The table** of basic daily data: heliogeophysical indices (W, F10.7, Xbcg, Sp, number of newly formed sunspot groups (N), MMP sector sign, relativistic electron fluence with E$>$ 2 MeV from space observatory GOES, preliminary average daily Ap-index according to the SWPC Service SWPC US, Dst-index and Ams - the average daily A-index according to the data of the IZMIRAN observatory;
- The section on the time of the start and duration of **fluxes of relativistic electrons with E$>$2 MeV** in geostationary orbits of high and extreme levels and the forecast for the next week.
- The level of **geomagnetic activity** for each day and the characteristics of mag-

netic storms recorded during the period under review (intensity on the scale of disturbances, A * -index of the magnetic storm and its duration) according to the data of IZMIRAN and the center of the SWPC US Service in Bolder, and the forecast of geomagnetic disturbances for the next a week.

Table 2. The scale disturbances of the environment space (Cosmic weather) for the epochs of increased, lowered SA and transitional periods (based on http://www.swpc.noaa.gov/sites/default/files/images/NOAAscales.pdf).

Impact on environment space			Epoch of environment space SA	Transition period (at 23 SC)	Epoch of lowered CA (24 SCs)
Level	Disturbances	Quantity	Frequency in	Frequency in	Frequency in
R: Electromagnetic shock: maximum X-ray flare class (wt/m^2)					
R5	Extremal	X20 ($2{\cdot}10^{-3}$)	< 1	2	0.01
R4	Very strong	X10 (10^{-3})	8	4	0.1
R3	Strong	X1 (10^{-4})	175	115	~60
R2	Medium	M5 ($5{\cdot}10^{-5}$)	350	272	~100
R1	Low	M1 (10^{-5})	2000	1295	~700
S: Corpuscular shock: proton flux cE $\geq$ 10 MeV and Jr $\geq$ 1 cm$^{-2}{\cdot}$c$^{-1}{\cdot}$cp^{-1}					
S5	Extremal	10^5	Not yet observed		
S4	Very strong	10^4	1/epoch	3	0.1
S3	Strong	10^3	3–10	11	5
S2	Medium	10^2	25	37	7
S1	Low	10^1	50	38	31
S0	Low	10^0	~50	59	49
G: Plasma impact (geomagnetic disturbances): a three-hour Kp-index					
G5	Extremal	Kp=9	4	20	~2/epoch
G4	Very strong	Kp=8–(9–)	100	25	3
G3	Strong	Kp=7	200	90	14
G2	Medium	Kp=6	600	344	116

5. CONCLUSION

27 years of publications of solar active phenomena forecast and the state of environment space in IZMIRAN cover incomplete three cycles and, as it later

turned out, include a transition period (SC 22-23) between epochs of increased and lowered SA and 24 SC - first cycle second epoch of the lowered SA. Time has confirmed that the principles of forecasting, taking into account the laws of the development of SCs with regard to the SA epoch for spot-forming activity, the processes of interaction of magnetic fluxes in the AR and beyond for solar flare events and the time interval for the passage of CHs through geoeffective heliolatitudes for the main part of recurrent disturbances, taking into account the characteristics of the interplanetary disturbances, provide sufficient information for building preliminary forecasts of the first level. They must give the time for the beginning of the effect on the environment space to an accuracy of 1 day (for magnetic disturbances and increases in the flux of relativistic electrons), input data intervals for refining prognostic models of individual types of impacts and response of selected media to disturbances data (level 2 forecasts). For example, the predicted range of changes in Wolf's number $\Delta W = 20$, in most cases is sufficient for ionospheric and radio wave propagation models.

Of particular importance is the forecast of the period of flare energy release of the AR, for which practically all significant flares of large and medium class are realized in this AR. In the current SC, this period occurs 1 ± 0.5 days after the first signs of the appearance of a new EMF within the boundaries of the AR, which makes it possible to give a first warning about the onset of the period of large flares with a high probability (70-90%). It should be emphasized that this forecast is not a separate flare, namely the time interval of about 55 hours, when the bulk of outbreaks from the energy of the new FMF introduced into the AR will take place. It should be specially emphasized that our method does not allow us to predict the time and power of a single flare event in this series. The forecast of the impact of each of these series of flares on the environment space is estimated by the parameters and dynamic phenomena of a separate flare event.

Another limitation is the real difficulty of isolating a new significant EMF in complex compact ARs with large areas and in the AR near the limbs of the Sun. At the same time, this method was successfully tested during the flights of the GRANAT space observatory(protection of scientific instruments from large fluxes of energetic solar protons), GAMMA (turn to the Sun with the possibility of powerful solar flares with significant γ-radiation) and the CORONAS project (for the service observation of flare events).

REFERENCES

1. Ishkov, V.N. & Shibaev, I.G. Solar activity cycles: general characteristics and modern forecasting boundaries. 2006, Bull. of RAS: Physical series, 70, 10, 1439

2. Shibaev, I. & Ishkov, V. Investigation of the Statistical Characteristics of the Wolf Numbers Reliable Series: Signs of Solar Cycles Likelihood. 2012, 7th Scientific Conf. "Space, Ecology, Safety" - SES 2011. Sofia, Bulgaria. 297, ISSN 1313-3888

3. Ishkov, V.N. The periods of "lowered" and "increased" solar activity: observational features and key facts. Solar and solar-terrestrial physic. Ed.By Yu.A.Nagovitsyn, VVM, St. Petersburg, 2013, 111 (in Russian)/ http://www.gao.spb.ru/russian/publ-s/conf_2013/conf_2013.pdf

4. Ishkov, V.N. Characteristics of solar activity of a protracted phase of a minimum of 23 - 24 solar cycles. Cycles of activity on the Sun and on the stars. Ed. By V.N. Obridko, Yu.A. Nagovitsina, VVM, St. Petersburg, 2009, 57 (in Russian)

5. Ishkov, V.N. Emerging magnetic fluxes are the key to predicting large solar flares. 1998, Bull. of RAS, Physical series, 62, 1835 (in Russian)

6. Golovko, A.A. Areas of a new magnetic flux with rapid evolution. 1. The diagram "magnetic flux is the lifetime. 1986, Solar Data, 5, 48

7. Golovko, A.A. Relationship between the maximum magnetic flux and the lifetime of solar active regions. 1998, Astron. Rep., 42, 546

8. Obashev, S.O., Minasyants, G.S., Makarenko, N.K. The structure of the time series formed by outbreaks in individual groups of spots. Sat. Solar Activity, Ed. By T.B. Omarov. Almaty, "Science", 1973, 103 (In Russian).

9. Choi, Y., Moon, Y.-J., Choi, S. et al. Statistical Analysis of the Relationships among Coronal Holes, Corotating Interaction Regions, and Geomagnetic Storms. 2009, Solar Physics, Vol. 254(2), 311 [doi:10.1007/s11207-008-9296-3]

10. Joselyn, J.A., SESC methods for short-term geomagnetic prediction, in Solar Terrestrial Predictions: Proceedings of the Workshop at Meudon, France, June 18–22, 1984, Boulder, Colorado, NOAA, 1984, 404

11. McAlister, A.H., Dryer, M., McIntosh, P., et al. A quiet CME and a severe geomagnetic storm: 1994, Proceedings of the Second SOLTIP Symposium, Watanabe, April 14–17, 1994. 5, 191

12. Mayaud, P.N. Analysis of Storm Sudden Commencements for the Years 1868-1967. 1975, JGR, 80(2), 111 [doi: 10.1029/JA080i001p00111] https://pdfs.semanticscholar.org/ 2b00/96b9264790cbeb00711027c99955ef6e26da.pdf

13. Ishkov, V.N. The Emergence Magnetic Fluxes and Flare Phenomena on the Sun. The Cand. Sci. (Phys.–Math.) Thesis, Troitsk, Moscow: N.V. Pushkov Institute of Terrestrial Magnetism, Ionosphere, and Radio Wave Propagation, RAS, 2008, 153 (in Russian)

GÜNƏŞ FƏALLIĞININ YERƏTRAFI KOSMİK FƏZAYA TƏSİRİ VƏ ONUN PROQNOZLAŞDIRILMASI

V. N. İşkov

Rusiya Elmlər Akademiyası, N. V. Puşkov adına Yer Maqnetizmi, İonosferin və Radiodalğaların Yayılması İnstitutu

Son onilliklərdə Günəşdəki fəal hadisələrin tədqiqi heç bir şübhə doğurmur ki, Yerətrafı Kosmik Fəzanın (YKF) halı və bütün əhəmiyyətli qısamüddətli həyəcanlaşmaları, Günəşdəki alışma hadisələri və Günəş tacının planetlərarası fəzaya açıq maqnit sahəsi oblastları (tac dəlikləri) ilə müəyyənləşir. Yeni yüksələn maqnit selinin artıq mövcud maqnit sahələri ilə qarşılıqlı təsiri fəal oblastlarda Günəş alışmalarına və bu oblastlardan kənara günəş liflərinin atılmasına səbəb olur. Yeni maqnit selinin yüksəlməsinin müşahidəsi, onun ədədi qiymətinin və yüksəlmə tempinin qiymətləndirilməsi, günəş alışmalarının və lif atılmalarının proqnozlaşdırması, onların geoeffektivlik dərəcəsinin müəyyənləşdirməsi baxımından faydalıdır. Günəş tacında alışmalardan və liflərdən həyəcanlaşmaların yayılmasını əks etdirən əsas agent tac kütlə atılmalarıdır ki, bu xususiyyətlər ideal şəkildə geomaqnit sahənin mümkün həyəcanlaşmasını, YKF-da yüksək enerjili yüklü zərrəciklər selinin mümkün artmasını qiymətləndirməyə imkan verir. Günəşdə geoeffektiv fəal hadisələrin və onların YKF-ya təsirlərinin müvəffəqiyətli proqnozu üçün günəş fəallığının cari tsiklinin və dövrünün inkişafını və xüsusiyyətlərini nəzərə almaqla son 3 gün ərzində Günəşdəki vəziyyəti bilmək lazımdır.

Açar sözlər: Fəal günəş hadisələri - Kosmik hava - Günəş fəallığının proqnozu - Yerətrafı kosmik fəzanın halının proqnozu

INVESTIGATION OF THE ATMOSPHERE OF THE STAR HR8120 (A8II)

Z. A. Samedov [a,b*]

[a] *Baku State University, Baku, Azerbaijan*

[b] *Shamakhy Astrophysical Observatory named after N.Tusi, Azerbaijan National Academy of Sciences, Shamakhy region, Azerbaijan*

The atmosphere of the giant star HR8120 (A8II) was studied by the atmospheric model. On the base of the observation, comparison of the theoretical values of the photometric indexes $[c_1]$,Q and application of the parallax the effective temperature T_{eff} of the star and the acceleration g of the gravitational forces were determined on the surface: $T_{eff} = 7880 \pm 150K, logg = 2.6 \pm 0.2$. Basing on the FeII lines the velocity of the micro-turbulent motion is determined:$\xi_t = 4.2$ km/sec.The amount of iron element is calculated in the atmosphere of the star and is compared with the value in the Sun the amount of iron element is determined by comparing the observable and theoretically calculated values of the equivalent widths of the FeII lines. The amount of iron element is obtained approximated to the amount in the Sun: $\log \varepsilon(FeII) = 7.65 \pm 0.2$.

Keywords: Fundamental parameters-stars – Chemical composition-stars – Personal-HR8120 (A8II)

1. INTRODUCTION

Chemical composition is one of the important parameters of the stars. The internal structure of the star and the radiation spectrum depend on the chemical composition. By determining the chemical composition, information may be obtained about the physical characteristics not only for the selected star and about the star systems, where this star belongs.The determination of the chemical composition of the stars is an important problem in the solution of the problems such as the formation of chemical elements, evolution of stars, the formation of the universe and its chemical evolution.

* E-mail: zahir.01@mail.ru

There is a process of deep mixing of the substances in the supergiant and giant stars.Ultimately the elements that are synthesized in the nuclei of these stars are transmitted into their atmosphere and the chemical composition of the atmosphere changes. In this regard, the definition of the chemical composition of the supergiant stars is an actual problem.

According to the modern evolutionary theory of the stars, as a result of the complete mixing of the substances in the giants from the spectral classes A, F, G, CNO-cycle products should be brought into the atmosphere of these stars and the amount of the elements C, N and O in the atmosphere should be changed. In the atmosphere of the supergiant and giant stars A, F, G the less amount of the carbon dioxide, the extra amount of nitrogen and a little less amount of oxygen have to be observed. The study of the chemical composition of the supergiant and giant stars atmosphere is one of the topical problems of astrophysics to confirm the accuracy of the theory of modern evolution (anomaly in the amount of the elements C, N and O).

Boyarchuk and Lyubimkov [1] discovered that, in the atmosphere of the supergiant stars of the spectral classes A, F, G among the variation of the elements C, N and O in the amount the additional amount of the element Na is observed. The reason for the excess of the element Na may be explained by the transformation of neon into the sodium in a Nena-cyclic reaction.

As a result of the complete mixing of substances in supergiant stars A, F, G, the element Na must be brought into the atmosphere of these stars and the amount of the element Na in the atmosphere should be changed. Thus, the determination of the amount of the element Na in A, F, G supergiant stars atmosphere is an important issue from the point of view of chemical evolution of these stars.

The fundamental parameters of the stars - effective temperatures and the determination of the acceleration of the gravity force on the surfaces are one of the important problems of astrophysics. The basic parameters for the effective temperatures and acceleration of the gravity force are the principle parameters for the atmosphere models, and the evaluation parameters for the stars - masses, radius, brightness, and age are determined by knowing these parameters.

The analysis of microturbulencity in the supergiant star atmosphere is of interest to verify the accuracy of the calculations of the theory of acoustic waves. For example ,Edmunsun estimates [12] show that in the atposhere of the yellow supergiant stars, the square average amplitude of velocity waves ϑ_ω is consired as an observed velocity of the micro-turbulent motion ξ_t.

There is still no generalized physical theory of the microturbulance in the atmosphere of the stars. The analysis of the microturbulancity is the actual issue of astrophysics for two reasons. First, to understand the physical nature of the

microturbulance, secondly, it is necessary to know the speed of the microturbulent motion in order to determine the chemical composition of the stars.

In this study, the atmosphere of the star HR8120 (A8II) is investigated: the effective temperature of the star and the acceleration of the gravity force and metallic level is determined. In our next investigations, it is envisioned to determine the amount of the light elements that have a chemical evaluation in this star. The observation material of the star was purchased in CCD-matrix spectroscopy at the Kassegren Focus of the 2M telescope of Shamakhy Astrophysics Observatory in 2014. DECH software packages were used to process the spectrum. The Atlas was drawn, measured and the equivalent width of spectral lines was measured.

2. ATMOSPHERE PARAMETERS: EFFECTIVE TEMPERATURE, ACCELERATION OF THE GRAVITY FORCE

The effective temperature and acceleration of the gravity force in the surface of the star is determined by the application of the model method and parallax. Model method uses the following criteria:

1. Comparison of the measured and theoretically calculated values of the index $[c_1]$.

In the $uvby\beta$ photometric system, the index $[c_1]$ is designated by the expression $[c_1] = c_1 - 0.2(b-y)$.This quantity is free from the influence of the absorption in the interstellar space. Since when one defines the fundamental parameters of the stars it is advisable to use the index $[c_1]$.

2. Comparison of the measured and theoretically calculated values of the index Q.

In UBV photometric system the index Q is designated by the expression Q=(U-B)-0.72(B-V). The quantity Q is free from the influence of the interstellar absorption. The observation values of the quantities $[c_1]$, Q is obtained by using the catalog of observation values [8]. To calculate the theoretical values of the quantities $[c_1]$,Q [7] is used. Based on the above criteria the $\log g - T_{eff}$ diagram is constructed (Fig. 1).

3. The application of parallax is considered as a new method for determining the effective temperature and acceleration of the gravity force of the stellar stars. Parallax application for the determining the effective temperature and acceleration of the gravity force of the stars for the first time was used in the Crimean Astrophysics Observatory [10], and the essence of the method is broadly interpreted in that article.

This method is very convenient because it does not depend on the choice of the atmospheric model. The right hand side of the known equation

$$\log g - \log M/M_{\odot} - 0,4BC - 4\log T_{eff} = -10,50 + 2\log \pi'' + 0,4m_{\upsilon} - 0,4A_{\upsilon}$$

is a quantity that can be defined from the observation for the considered star and the left hand side is a quantity that depends on T_{eff} and $\log g$. Giving different values to T_{eef} and logg one can define $M \setminus M_{\odot}$ from the evaluation curves [6], and from the star atmosphere models. The pairs T_{eff}, $\log g$ are defined and shown in the diagram $\log g - T_{eff}$ (Fig. 1). The parameters of the star can be

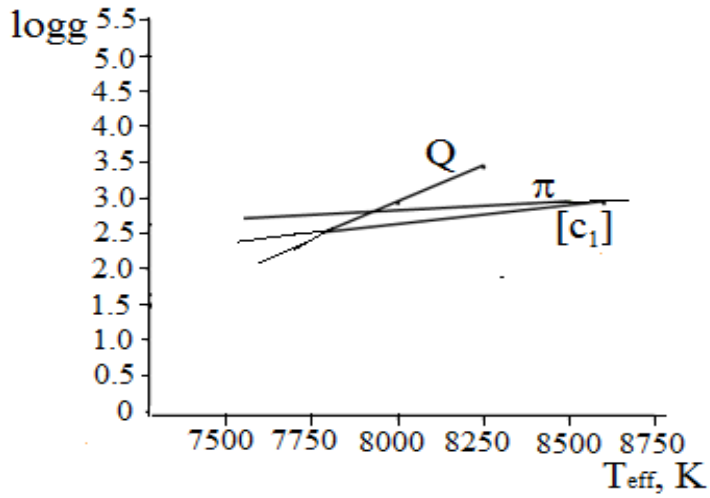

Fig. 1. The diagram that defines the T_{eff} and logg parameters of the star HR8120 (A8II)

defined from (Fig1) as follows:

$$T_{eff} = 7880 \pm 150K, \log g = 2.6 \pm 0.2.$$

3. MICROTURBULENT MOTION VELOCITY, AMOUNT OF IRON ELEMENT

In the atmosphere of the star, the microturbulent velocity ξ_t and amount of the iron is determined by the FeII lines. To determine the microturbulent motion velocity ξ_t atom or ion of any element one must have a large number of lines containing a wide range of W_{λ} diameters. The microturbulent motion velocity ξ_t is chosen so that the amount of the elements assigned by different lines does not change with the increasing the equivalent widths W_{λ}.

The most lines in the spectrum of the star we study are the FeI lines, and then FeII lines. However, the effect of the variations LTT over FeI lines is strong. In the case of LTT, the velocity of the microturbulent motion determined on the FeI lines is less than the velocity determined by FeII lines. When the calculations are carried out for the LTT case, the amount of iron determined on the FeI lines is lower than the amount determined without LTT. For the first time, Boyarchuk et al. [2] obtained this result for supergiant stars of the F spectral class. Later on, the F and G spectral class stars were approved by other authors [11]. Unlike the FeI lines, there is no effect of the variations of LTT on the FeII lines. In the atmosphere of the star, FeII lines are used to determine the microturbulent velocity ξ_t.

As L. Lyubimkov and Z.A. Samedov [10] show, the velocity ξ_t of the microturbulent motion increases as the altitude in the atmosphere of the stars of the spectral class F increases. The effect is stronger as stronger the line. For the weak lines, this dependency can be ignored and it is assumed that the velocity ξ_t of the microturbulent motion is constant in the star's atmosphere.

When determining the microturbulent velocity ξ_t only weak enough lines are used. These lines are formed in the deep layers of the atmosphere; these layers are parallel and are in the form of LTT.

The amount of iron $\log \varepsilon(FeII)$ is calculated by giving different values for the microturbulent motion velocity ξ_t based on the Kurucz model [5] with parameters $T_{eff} = 7880K, \log g = 2.6$. The amount of iron is determined by comparing the observable and theoretically calculated values of the equivalent widths of the FeII lines.

The atomic data of the spectral lines were taken from the database VALD-2 [4]. If $\xi_t = 4.2$ km/sec then there is no correlation between $log\varepsilon(FeII)$ and W_λ Fig. 2.

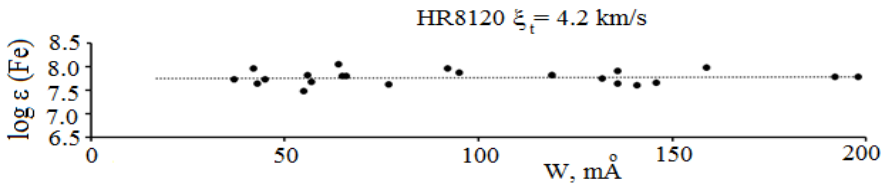

Fig. 2. Determination of the velocity ξ_t of the microturbulent motion

Note that the quantity [Fe/H] ([Fe/H] = Log= $log_*(Fe) - log\varepsilon_\odot$(Fe)) is the "metallicity" indicator of the stars. Here $log\varepsilon_\odot$ (Fe) is an amount of iron in the Sun: $log\varepsilon_\odot$ (Fe)=7.45 [3]. [Fe/H]=7.65-7.45=0.2. This is one of the fundamental

parameters of the stars, since the quantity [Fe/H] quantifies the amount of metals in the substance that the star is formed. Knowing the quantity [Fe/H], it is determined that the star and the Sun consist of the substance with same or different "metallicity".

Study of the "metallicity" in dependence on the distance from Galactic center, is an actual research that is of great scientific importance in solving problems such as the settling of the stars, the formation of the chemical elements.

Thus the parameters of the star:

$$T_{eff} = 7880 \pm 150K, logg = 2.6 \pm 0.2, \xi_t = 4.2km\ s^{-1},$$

$$log\varepsilon(Fe) = 7.65, [Fe/H] = 0.2.$$

The amount of metals in the star is close to their amount in the Sun. This shows that the giant star HR8120 (A8II) and the Sun are formed from the same substance. This result is a significant consequence of the Galactic chemical evolution model.

4. MAIN RESULTS

1. By the application of the model and parallax the effective temperature T_{eff} and acceleration g of the gravity force on the surface of the star HR8120 (A8II) is determined as follows: $T_{eff} = 7880 \pm 150K, logg = 2.6 \pm 0.2$.

2.On the base of the lines FeII the velocity of the motion in the star atmosphere is determined: $\xi_t = 4.2km\ s^{-1}$.

3. The amount of iron element was determined in the atmosphere of the star, and compared with the amount in the Sun. It has been discovered that the amount of iron element in the star is close to the amount in the Sun.

REFERENCES

1. Boyarchuk, A.A., Lyubimkov, L.S. 1983, Izv.Kr.AO, 66, 131 (in Russian)

2. Boyarchuk, A.A., Lyubimkov, L.S., Sahibullin, N.A. 1985, Astrophysics, 22, 203. (In Russian)

3. Scott, L.S., Asplund, M., Grevesse, N., Bergemann, M., Sauval, M. The elemental composition of the Sun II. The iron group elements Sc to Ni. 2015, A&A, 26, 573 [doi: 10.1051/0004-6361/201424110]

4. Kupka, F.N., Piskunov, T., Ryabchikova, T., Stempels, H.C., Weiss, W.W. VALD–2: Progress of the Vienna Atomic Line Data Base. 1999, A&AS, 138, 119 [doi: 10.1051/aas:1999267]

5. Kurucz, L.S. CD-ROM 13, ATLAS9 Stellar Atmosphere Programs and 2km/s grid. Cambridge, Mass.; Smithsonian Astrophys.Obs. 1993

6. Claret ,A. New grids of stellar models including tidal-evolution constants up to carbon burning.I.From 0,8 to 125 M at Z=0.02. 2004, A&A, 424, 3, 919 [doi: 10.1051/0004-6361:20040470]

7. Castelli, F., Kurucz, R.L, Piskunov, N.E., Weiss, W.W., Gray, D.F. Eds. Proc. IAU Symp. 210, Modelling of Stellar Atmospheres. Poster A20. 2003, Astron. Soc. Pac., San Francisco, A20

8. Hauck, B., Mermilliod, M. uvbybeta photoelectric photometric catalogue. 1998, A&AS, 129, 431 [doi: 10.1051/aas:1998195]

9. Lyubimkov, L.S., Samedov, Z.A. Variability of the Microturbulence in the Atmospheres of F Supergiants. 1990, Astrophysics, 32, 30

10. Lyubimkov, L.S., Lambert, D.L., Rostopchin, S.I., Rachkovskaya, T.M., Poklad, D.B. Accurate fundamental parameters for A-, F- and G-type Supergiants in the solar neighbourhood. 2010, MNRAS, 402, 1369 [doi: 10.1111/j.1365-2966.2009.15979.x]

11. Thevenin, F., Idiart, T.P. Stellar Iron Abundances: Non-LTE Effects. 1999, ApJ, 521, 753 [doi: 10.1086/307578]

12. Edmunds, M.G. A model for stellar microturbulence. 1978, A&A, 64, 103

HR8120 (A8II) ULDUZ ATMOSFERININ ÖYRƏNILMƏSI

Z.A. Səmədov[a,b]

[a] *Bakı Dövlət Universiteti, Bakı, Azərbaycan*
[b] *N.Tusi adına Şamaxı Astrofizika Rəsədxanası, Azərbaycan Milli Elmlər Akademiyası, Şamaxı rayonu, Azərbaycan*

Atmosfer modeli üsülu ilə HR8120 (A8II) nəhəng ulduzunun atmosferi tədqiq edilmişdir. $[c_1]$, Q fotometrik indekslərinin müşahidə və nəzəri qiymətlərini müqayisəsi və parallaksın tədbiqi əsasında ulduzun effektiv temperaturu T_{eff} və səthində ağırlıq qüvvəsinin təcili g təyin edilmişdir: $T_{eff} = 7880 \pm 150K, logg = 2.6 \pm 0.2$. FeII xətlərinə əsasən mikroturbulent hərəkət sürəti təyin edilmişdir: $\xi_t = 4.2$km s^{-1}. Ulduzun atmosferində dəmir elementinin miqdarı hesablanmışdır və Günəşdə olan miqdarla müqayisə edilmişdir. Dəmir elementinin miqdarı FeII xətlərinin ekvivalent enlərinin müşahidədən ölçülmüş və nəzəri hesablanmış qiymətlərinin müqayisəsi əsasında təyin edilmişdir. Dəmir elementinin miqdarı Günəşdə olan miqdara yaxın alınmışdır: $\log \varepsilon(FeII) = 7.65 \pm 0.2$.

Açar sözlər: Ulduzlar: fundamental parametrlər - Ulduzlar: kimyəvi tərkib – Ulduzlar: fərdi - HR8120 (A8II)

LIGHT CURVE ANALYSIS OF DN TAU

N. Z. Ismailov [*]***, S. A. Alishov, N. I. Gulmaliev***

Shamakhy Astrophysical Observatory named after N.Tusi,
Azerbaijan National Academy of Sciences, Shamakhy region, Azerbaijan

The results of photometric observations of the classical T Tauri type star DN Tau, performed at ShAO for 2016-2017, are given. By analyzing the summary light curve, it is shown that the seasonal changes in the brightness of the star in the V-band is 0.5 -1.0 mag. The average annual brightness values show variability with a characteristic time of about 25 years. An analysis of the change in the brightness of the star over different seasons allows to clearly detecting the 6-day period of the brightness variability, determined earlier by other authors. Variation in the period for various seasons differs by a few tenth day. It is shown that the seasonal phase light curves becomes obvious a shift in the phases of the maximum and minimum, and also the period changes by a few tenth day. It is assumed that the observed shift in phase and the change in the value of the 6-day period are related with the migration of spots and the differential rotation of the star's atmosphere.

Keywords: stars: formation – stars: pre-main sequence – stars: – individual: – DN Tau

1. INTRODUCTION

The star DN Tau was first noted in the work [1] – the $H\alpha$ review of Taurus clouds as a moderately active T Tauri type star. More detailed spectroscopic observations revealed emission lines of the Balmer H series, H, K Ca II lines and weak lines He I and Fe II, which are superimposed on the photospheric spectrum of the normal dwarf with spectral class M0. According to Herbig [2], the spectrum of the star is classified as M1Ve. A change in the equivalent width of the $H\alpha$ emission line for 1976-1981 was found from 12 to 7 Å([3], [4]).

Photometric changes in brightness were detected in the IR and optical range [5], where the amplitude in the V-band was 0.8 mag. Only in one case, brightness increase at 0.8 mag in the B-band in 35 minutes was reported [6], after which

[*] E-mail: ismailovn@yahoo.com

there were not observed a sudden changes in time interval 35 years. Bovier et al. [7] by using photometric and spectral observations, discovered a periodic change in brightness. The authors explained this change by the presence of a large cold spot on the star's surface. Moreover, the spot area varied from 9 to 36% at the spot temperature, below the photosphere temperature by 700 K. According to this data, no signs of a hot spot were found.

For the first time,by Verba et al. [8] during 15 days of photometric observations, 6.6 day periodic variability, and in the U band a phase shift at 0.47 was detected. This was interpreted by the existence of a hot spot, which is located near to a cold spot, the temperature of which is 500 K below the neighboring photosphere with an area of 20% of the surface. According to new data [9], is shown that the star maybe an intermediate type between the types of CTTS and WTTS. Also unclear whether the star is in the final stage of the disk evolution, or it is a temporary quiet state of activity.

In order to search for planets, in [10] spectral observations is carried out in the optical and infrared ranges. They showed that the radial velocity of the star is changing due to the spot on the surface. Observations from Einstein's satellite showed a characteristic change of 0.1 dex between 1980–1981 about an average value of the radiation 1030 erg/s [11], [12].

According to Donati et al. [13], the star has a photospheric temperature of 3950 $\pm$ 50 K, a luminosity of 0.8 $\pm$ 0.2 $L\odot$, a rotation period of 6.32d, an age of 2 $\cdot$ 106 years, a radius of 1.9 $\pm$ 0.2 $R\odot$, and the axis of rotation is at an angle to the observation of 35 $\pm$ 10°. Spectral and photometric observations show that DN Tau is a typically quiet T Tauri star. According to observations, the star has an amplitude of brightness variability peak of 0.15 mag and a period of rotation of the star of 6.43 days [14]. According to Fourier analysis [15], a period of 6 days was obtained. On periodograms are observed a sharp peak of 6.28 days.

The physical parameters of the star are determined uncertainly due to the inaccurate determination of the spectral class and class of luminosity, and also a big error in determining the magnitude of interstellar reddening. So, according to data [3], the star has Av = 0.42 $\pm$ 0.16 and the spectral class M0. Bouvie et al. [7] showed that Av = 0.3 $\pm$ 0.1 and the star is located on the edge of the cloud in which it was formed.

In [13], the following star parameters from spectropolarimetric observations is obtained: Teff = 3950 $\pm$ 50 K, log g = 3.7 4$\pm$ 0.1, L = 0.8 $\pm$ 0.2 $L\odot$, P = 6.32d, R = 1.9 $\pm$ 0.2 R, M = 0.65 $\pm$ 0.05 $M\odot$, the angle between the line of sight and the rotation axis is i = 35 $\pm$ 10° and the age is 2 $\cdot$ 106 years. The authors was detected a circular polarization, both in photospheric lines and emission lines, forming in the accretion zone, which testify the existence of a magnetic field above 1.8 kG.

On the results of these studies, we suppose a change in the observed value of the period DN Tau for different seasons. For research of the character of observed photometric period of the star, additional observation programs are needed. The purpose of this work is a photometric research of the star on our observations and on the data obtained from archives.

2. OBSERVATIONAL MATERIAL

2.1. Observations at ShAO

Our observations were carried out on the Cassegrain focus of the Zeiss-600 telescope by using the single-channel photometer operating with a set of standard BVRIc filters. A detailed description of the technical characteristics of the system telescope + photometer was given in [16]. In our observations, a CCD FLI 4096x4096 was used. The working field of the frame was 17 angular minutes. We are tried keeping the observational objects and standards closer to the center of the frame. The accumulation time in different filters ranged from 30 to 90 seconds. Such a choice of timing of the accumulation was bound partly due to the uneven behavior of the clock mechanism of the telescope. 5 frames were received in each filter, the maximum accumulation signal for software star and standards made up 30000-40000 ADU. To increase the signal-to-noise ratio S/N, the obtained frames were summed over individual filters. The summation was also carried out for a flat field, a dark signal and frames of bias.

In Fig. 1 is shown a frame of the area of the star DN Tau. Here the designations are as follows: V-variable, K1, K2-control stars, S-standard. For the selection of the star with the most stable brightness and for further use as a standard and control stars, trial combinations were performed. Wherein, at first one star was used as a standard, the rest were determined relative to it. Then the standard stars were replaced by other stars of the field and the magnitude of the relatively new standard was again determined. In conclusion, the star that gives the smallest value of the standard deviation of the magnitude in this band was chosen as the standard. Our data for 35 individual nights of observations showed a standard deviation from the average for different filters, the following values for standard and control stars: σR = $\pm$0.018m, σB = $\pm$0.015m, σV= $\pm$ 0.021m. In this work, for analysis, we used the instrumental magnitude of the V- brightness values. Binding to the international system was not carried out, so we are following only the relative change in the magnitude of the star in the instrumental system. As a standard, eventually the star GSC 01829-00150 (2MASS J04351894 + 2415374) was selected with a value brightness of V = 13 mag. Table 1 shows

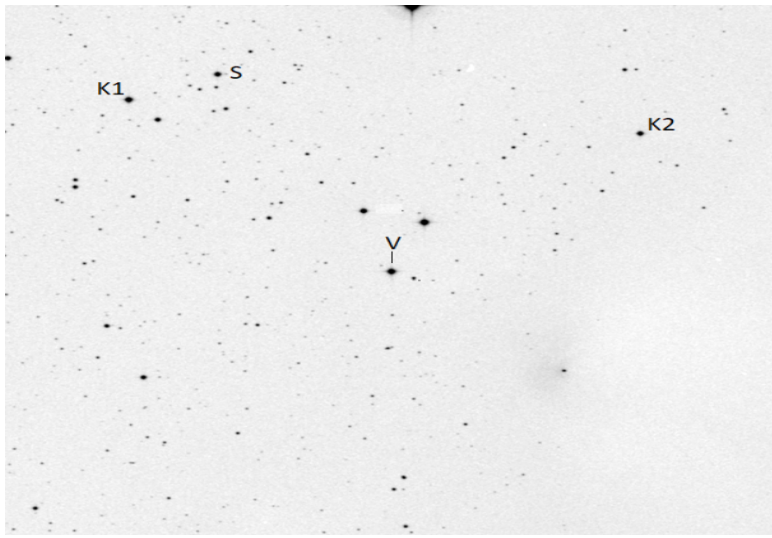

Fig. 1. Identifying map of the star DN Tau. I was marked: V- variable, K1, K2 control stars, S-standard star.

the results of our observations for 2016–2017 in different filters. The magnitudes obtained in Table 1 given relative to the standard in the instrumental system.

2.2. Material selected from literature

We selected from different sources the results of photometric observations of the star for approximately 50 years of observations. Main part of the material was taken from the archive of the Wesleyan University covering the period of time 1962-2003 (491 points in total, by program ROTOR), ([17], [18]), and also from the archive of the automatic telescope ASAS [19] (http: // www.astrouw.edu.pl/asas/), received for 2003-2009 (379 points in the V-band). Full brightness data, including our results, contains more than 900 points in the V-band. Despite the long observation period, the results of the ROTOR program can be considered a homogeneous material, since the overwhelming majority of observations here, done by one group of observers in Uzbekistan. Average error of these measurements in the V band is about $\pm$ 0.01mag. Our data is also defined about the same accuracy. The accuracy of the ASAS data is about twice as bad as other measurements. Nevertheless, the amplitude of seasonal changes of brightness is quite large, so the data allow analyzing the overall picture of changes, not considering possible systematic differences in observations.

Table 1. The results of the observations of DN Tau in SHAO

JD	R	B	V
2457721.349	11.546	13.742	12.423
2457722.231	11.57	13.704	12.436
2457723.247	11.476	13.417	12.269
2457743.234	11.406	13.433	12.256
2457745.334	11.42	13.481	12.287
2457745.377	11.393	13.475	12.233
2457746.372	11.464	13.447	12.268
2457749.256	11.414	13.388	12.242
2457751.258	11.447	13.478	12.266
2457755.33	11.42	13.363	12.244
2457756.263	11.496	13.561	12.354
2457757.278	11.514	13.358	12.296
2457757.298	11.54	13.412	12.322
2457758.134	11.45	13.418	12.255
2457758.154	11.459	13.471	12.284
2457758.177	11.455	13.489	12.311
2457759.293	11.555	13.647	12.417
2457759.314	11.567	13.618	12.393
2457760.263	11.598	13.536	12.401
2457760.287	11.524	13.506	12.256
2457771.273	11.455	13.307	12.235
2457771.297	11.42	13.375	12.207
2457777.25	11.463	13.408	12.302
2457777.27	11.416	13.405	12.256
2457777.292	11.453	13.382	12.272
2457804.256	11.607	13.736	12.501
2457804.273	11.605	13.753	12.439
2457805.34	11.554	13.737	12.503
2457805.36	11.57	13.741	12.459
2457806.368	11.524	13.627	12.393
2457814.232	11.519	13.712	12.418
2457814.256	11.546	13.701	12.389
2457849.142	10.926	12.036	11.486
2457997.485	11.557	13.77	12.47
2457998.41	11.677	13.802	12.697
2458071.192	11.62	13.686	12.505
$Sigma$	0.1201024	0.292019	12.32625
$mean$	11.489611	13.50339	0.179585

3. MAIN RESULTS

In the Fig. 2 was shown a summary light curve of the star constructed by all collected observational data. As it can be seen, inside the season the brightness variation of the star is from 0.5 mag to 1 mag. The average annual value of brightness also changes smoothly. The data from 1962-2003 show the existence of slow increase of the brightness to a maximum, and subsequent observations of a

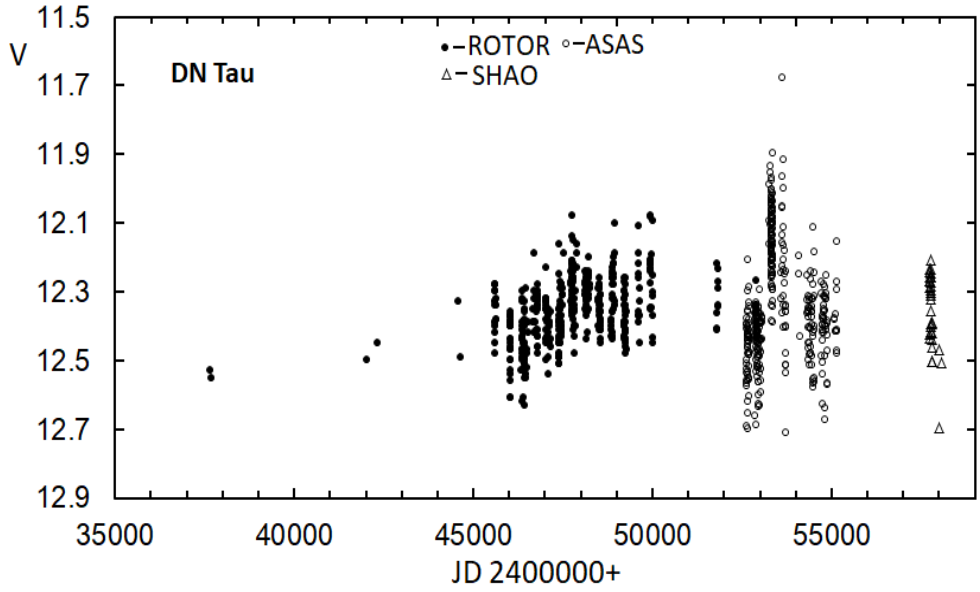

Fig. 2. The master light curve of the star DN Tau. Dark cycles, is from ROTOR program data, light circles – ASAS, triangles,- ShAO.

slow decreasing. The total characteristic time of a change in average magnitude brightness is not less than 10000 days.

Another one feature on the star's light curve is received per ASAS data. As seen, mid-seasonal value of brightness in different years, differ greatly in different years. The reason of such distinction is not quite clear. Perhaps in different years, the activity of the star is changing significantly.

3.1. Brightness distribution diagrams

For the analysis, we plotted diagrams the brightness distribution of the star in each of the UBVRI filters according to the ROTOR program. For compliance homogeneous in statistical diagrams, data from other sources were not used. In Fig. 3 the obtained diagrams of the brightness distribution of the star in

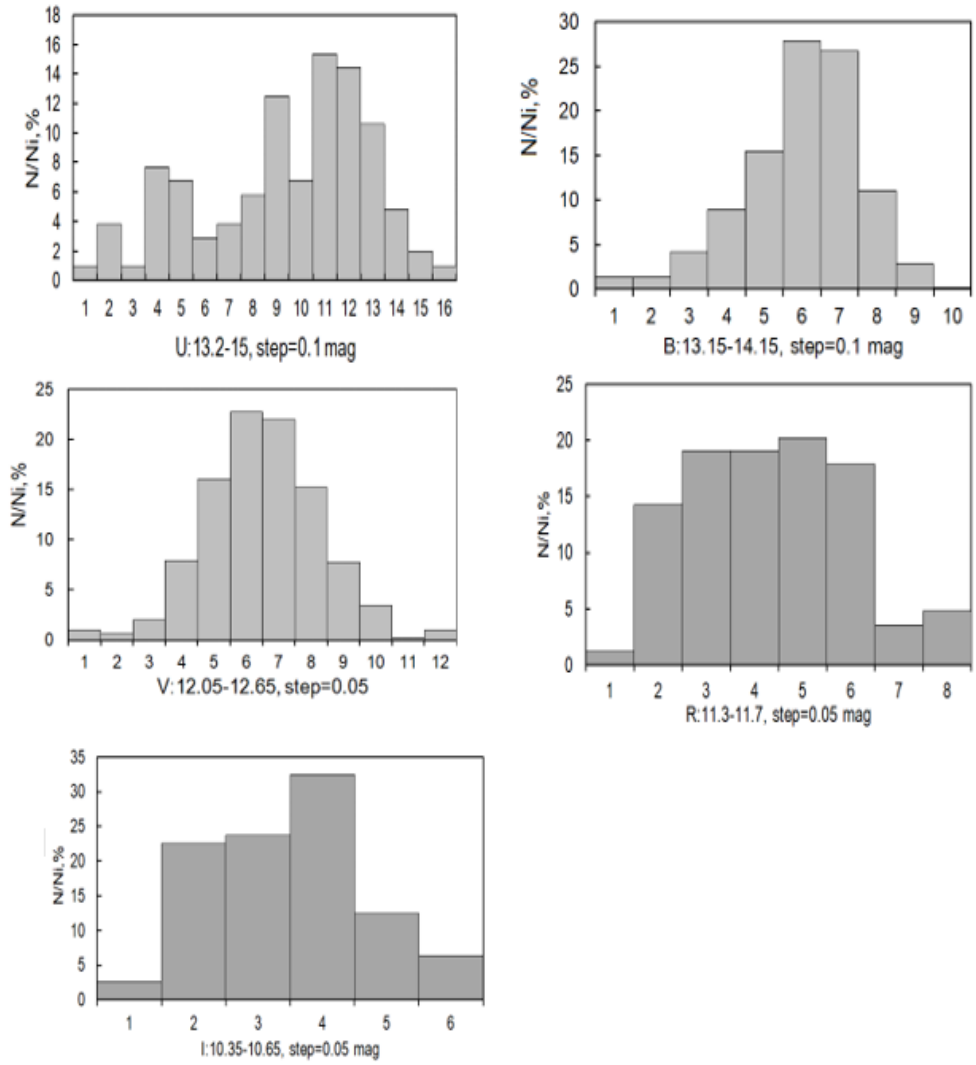

Fig. 3. The brightness distribution in UBVRI bands of DN Tau. On the abscissa was presented the interval of brightness variation and the step of ranges. On the ordinate was presented the number of given brightness state relative to all number of brightness in percent.

different photometric bands are shown. Here in each diagram on abscissa the interval of brightness variation and the step is given, over which the distribution from maximum to minimum is composed, and on ordinate the relative number N/Ni in percent. As seen from Fig. 3, for the V-band distribution of the diagram the brightness has mainly symmetric form. Total interval of changes in brightness and amplitude of changes in the V- band is, respectively, V: 12.05–12.65

mag, $\Delta V = 0.6$ mag. In the bands U and B, a significant asymmetry is observed, which, apparently, occurs with a frequent flash-like increase in brightness. In the U and B bands, the interval of changes in brightness and amplitude of variation is, respectively, U: 13.2-15.0 mag, $\Delta U = 1.8$ mag, B: 13.15-14.15 mag, $\delta B = 1.0$ mag. In the bands R and I, the distribution of brightness has approximately the same character. In these bands, the variability interval and the amplitude of the brightness changes are respectively: R: 11.3-11.7 mag, $\Delta R = 0.4$ mag, I: 10.35 mag-10.65 mag, $\Delta I = 0.3$ mag. In these bands, the amplitude of the change in brightness is minimal, and the distribution of brightness shows stability in a considerable interval. In Fig. 4 the diagrams of changes in the color indexes of U-B, B-V and V-R versus V-band brightness variation are shown. Quantity of observations in the U-band is less, and from the diagram can be see that, there is not detected definite relation between the U-B color index and V-brightness.

The B-V and V-R color-indexes change weakly from brightness, so since the star brighter in the V-band, then brighter also the appropriate color-index. Besides, in depending V – R versus V, are observed two groups of points that are significantly displaced relatively apart. The reason for such discrepancies is complicated to explain. It could be due with significant change in color in the red band, when will be passing component in a binary system, or large protoplanet, moving in Keplerian orbit around the star.

3.2. Fourier analysis of the light variability

In Table 2 is given the results of the works by detected of the 6-day period on the light variability and on the spectrum of DN Tau. In the first column of the table is given the value of obtained period, in the second column the definition error, the third one is the used method, fourth is the authors. As seen from Table 2, the periods obtained by different authors differ each from other for a few tenth day. Therefore, there is a need to check, whether a change in the value of this period, occurs, and if so, what is the reason for such changes of period. For research this task, we have performed a search for period by data individual seasons of observations.

For perform a search, periodic changes in brightness of the star, was used Scargle method [20] and further modified and applied in works [21] and [22]. Scargle method allow to compute false value of frequency the probability F for any peak, taken from the power spectrum, i.e. likelihood that it will be more “white noise” than required value. The probability that the data contain one periodic signal is equal 1-F. If we calculate the normalized power spectrum z for independent fre-

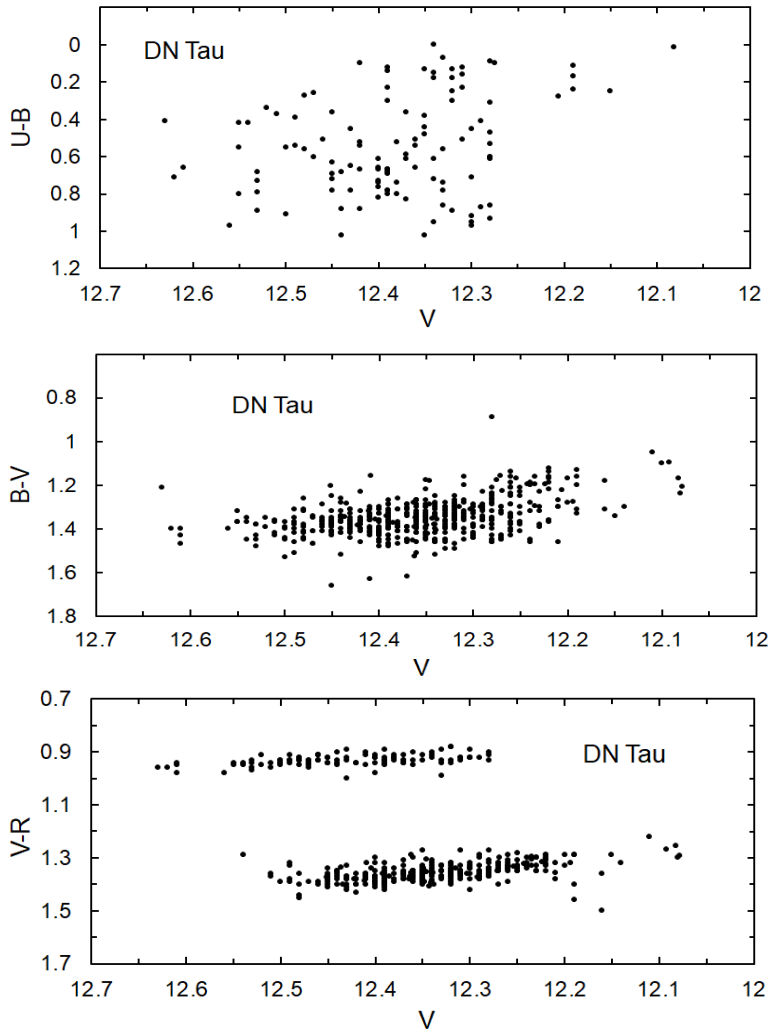

Fig. 4. The diagrams of color-indexes U-B, B-V and V-R versus V-brightness.

quencies, then for a non-equal-standing series, the parameter F may be computed by the well-known expression

$$F = 1 - (1 - e^{-z})^{n_i}.$$

Maximum frequencies interval at such search determined by ratio υ max $= 1/2\Delta t_{min}$, where Δt_{min}- is the minimum span of time between neighboring observation points. The choice of program is due to the fact, that this program is applied for an array with an uneven time series. As a rule, in astronomical observations we often deal with arrays of data with unequal by time, intervals.

Table 2. The results of the observations of DN Tau in SHAO

Period (days)	σ	**method**	$V \sin i(kms^{-1})$	**author**
$P = 6.33$	0.20	IR spectroscopy	8 ± 2	Prato et al. 2008 [10]
$6.0 - 6.28$	0.05	photometry	12.3 ± 0.6	Vrba et al. 1993 [9]
6.6	0.1	photometry		Vrba et al. 1986 [8]
6.32		photometry		Artemenko et al.2012 [25]
6.22	0.10	spectropolarimetry	9 ± 1	Donaty et al.2013 [13]
6.43		photometry		Percy et al. 2006 [14]
6.0		photometry	8.1	Appenzeller et al.2005 [24]
		spectroscopy	12.3 ± 0.6	Nguyen et al.2012 [23]
6.0		photometry	8.1 ± 2	Bouvier & Bertout1989 [26]
$6.0 - 6.2$		photometry		Percy et al. 2010 [27]

For the test for DN Tau the stability of the 6-day variability period, we used V-band data, consisting of about 800 observation points. These data were collected in groups, containing data of individual years. From received groups for application of analysis, we chose those in which there are located at least 50 observation points. Total had been allocated 7 such arrays, satisfying this condition. In the received separate groups, we looked for frequencies in the interval from 0 to 0.5 d^{-1}. Power spectra and windows for individual groups were obtained. Figure 5, for example are given the power spectra for different data groups.

As seen in all the groups, the 6-day period of light variability easily stands out, which was by this time determined by different authors.

The result of the analysis for each groups is given in Table 3. For separate columns in Table 3, from left to right are given: name of the data groups, the number of points in the group, the most significant frequencies, magnitudes of the power spectrum, corresponding to these frequencies, and the values of the periods obtained in days.

As seen from Table 3, from 7 data groups, in 6 of them 6-day period of variability confidently was detected. The remaining probable periods are unstable and by different groups are not saved. We obtained a formal mid-statistical value of the period by different groups, as P = 6.231 $\pm$ 0.089 days. This value of the period agrees well, with period of variation of the longitudinal magnetic field strength of the star P = 6.22 $\pm$ 0.10 days, presented in the work [13].

Both the results of our analysis and other authors have shown that the value of the period of 6.3 days is not constant, and in different seasons differs by several tenths part of days (Tables 2 and 3). The reason for such differences may be the

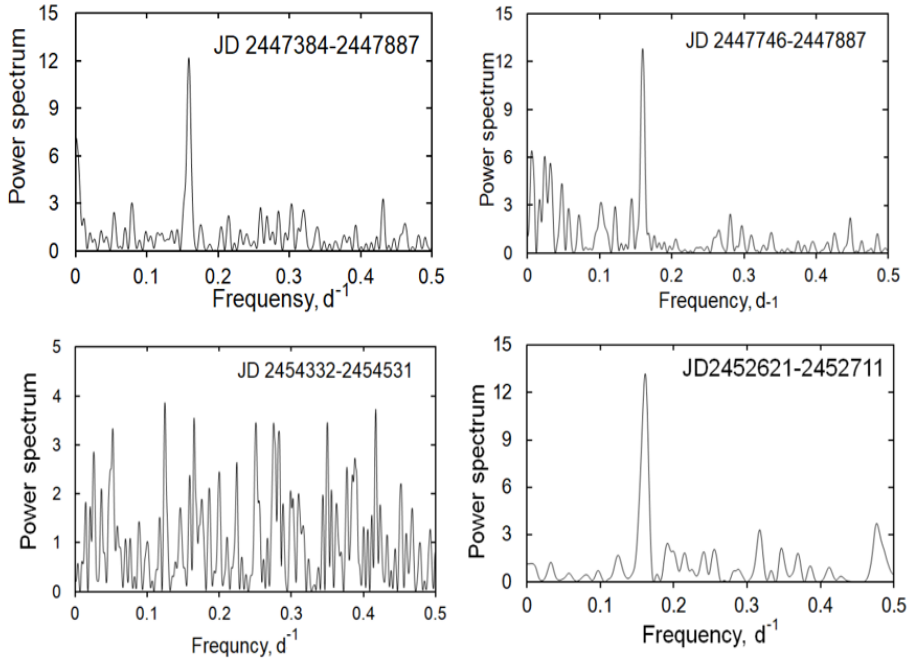

Fig. 5. Examples of power spectrum for different groups, for V-band brightness values. In all the figures, the presence of the 6-day period is well detected.

differential rotation of the atmosphere of the star in different latitudes and the migration of spots in latitude. Therefore, for more accurate period value we used our data rounded to tenths and more exact data.

3.3. Phase shifts in the period of 6.3 days

On the obtained value of the period, phases for each season of observations were calculated. Phases were calculated by elements Min V = JD 24546361.456 + 6.3 E. In Fig.6 is shown examples of phase curves for different seasons of observations in the V – band. As seen from Fig.6, phase light curves obtained in different seasons of observations, show a various level of scatter of points in phases. For example, data of the seasons presented on upper panels of Fig.6 have less scatter, than the data presented on the lower panels. The change in scatter level of points on seasonal light curves may be due the change, for example, the sizes of spots on the star's surface in different years. On lower left panel showed phase light curve, obtained according to our observation. Here with the contour selected 5 points, showing a significant deviation from the phase curve. Such a scatter of points sometimes is observed and in other seasons (see Fig. 6, upper right panel).

Table 3. Results of Fourier analysis of V-data for different seasons (groups).

Group name	N	f , day^{-1}	P	P , days
mas1	79	0.1590	14.253	6.289
		0.0884	6.370	11.312
		0.2263	5.750	4.419
		0.3300	5.440	3.030
mas2	57	0.1590	12.200	6.289
		0.4315	3.280	2.317
mas3	64	0.1595	12.821	6.270
mas4	54	0.1610	13.192	6.211
mas5	76	0.0485	4.221	20.619
		0.1595	5.688	6.270
		0.2525	5.574	3.960
		0.3175	6.169	3.150
mas6	93	0.0548	7.568	18.265
		0.0936	8.287	10.684
		0.1399	11.273	7.148
		0.3658	6.570	2.734
		0.4868	10.050	2.054
mas7	52	0.0260	2.860	38.462
		0.0525	3.335	19.048
		0.1245	3.865	8.032
		0.1650	3.548	6.061
		0.2510	3.455	3.984
		0.2755	3.453	3.630
		0.3500	3.461	2.857
		0.4140	3.731	2.415

Such a scatter of points most often occurs in phases 0.3 ± 0.7 and may arise due to flare activity of the star. In total, there 21 separate seasons of observations were selected, in which there is sufficient amount of points, allow satisfactorily describe full phase light curve. For all individual seasons were constructed the phase light curves and by them phases of the minimum and maximum of light

Table 4. Selected phases of maximum and minimum in seasonal phase V-light curve.

Middle date of season JD2400000+	Max Phase	Min phase
45621		0.304
46049		0.521
46440	0.829	0.326
46738		0.3
47093		0.3
47452	0.625	0.15
47814	0.797	0.262
48210	0.876	0.396
48538		0.505
48906	0.571	0.111
49247	0.555	0.08
49624	0.8	0.4
49985	0.28	0.743
52896		0.451
52664	0.813	0.131
53003	0.891	0.359
52666	0.802	0.239
52960		0.371
53313	0.489	
53669		0.437
54431	0.7	0.1
54806	0.7	0.1
55126		0.497

curves were determined. In Table 4 is shown the results of such selection of phases minimum and maximum obtained in different seasons. The time given in Table 4 corresponds to the middle between the dates of the beginning and end of the observation season. The absence of data in the table means, that due to less of data in this season, it was impossible to determine exactly from light curve the phases of the extremes.

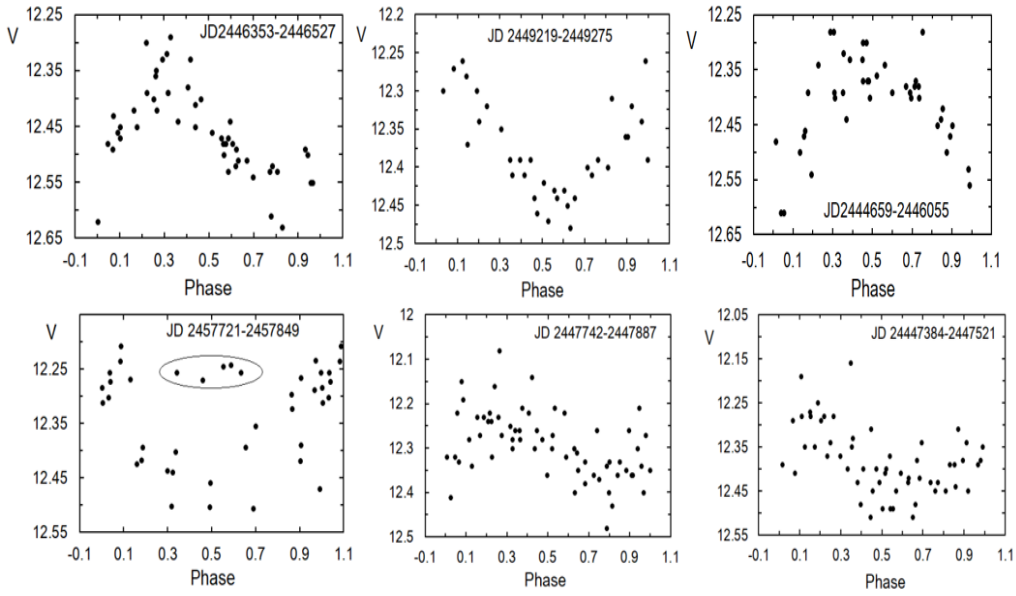

Fig. 6. Phase lights curves, obtained for different seasons of observations. Bottom left panel was obtained according to our observations, where points are selected contour significantly deviating from phase curve.

In Fig.7 is presented diagram of dependence the maximum and minimum phases in time for different seasons of observations. From this Figure is clearly shown that in different seasons of observations in the light curves the maximum and minimum showing a significant shift in phase. Shift value in phase of maximum or minimum points of light curve can reach up to before 0.7 R. With a rotation period constancy, such shift may be due to migration of spots on the surface by star longitude. Such a shift is well observed on separate phase light curves, which are shown in Fig. 6.

From the examples of seasonal light curves given in Fig.6 it's seen, that in the individual seasons of observations noticeably varied the rate of change of the brightness. For estimate brightness gradient during the period (by phase) in different seasons, we have selected 10 most complete light curves, which simultaneously well is stands out phases the maximum and minimum. In Table 5 is giving a list of selected groups, JD - dates of the middle of season, dφ - phase difference between phases of maximum and minimum, dm - difference of star magnitude, respectively, in the phases of maximum and minimum and | dm/dφ | - the module of rate change of star magnitude between phases of the maximum and minimum.

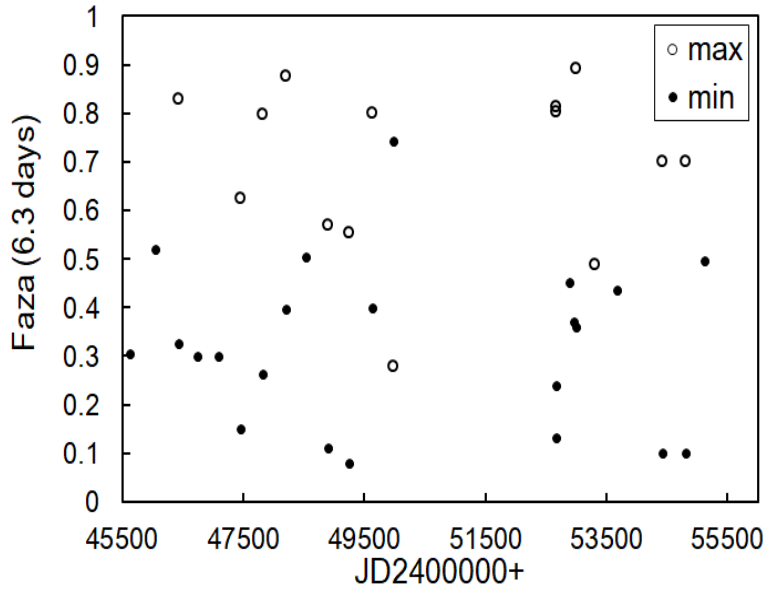

Fig. 7. The phase variability of maximum (light cycles) and minimum (dark points) of the brightness in time. The time in JD on the abscissa axis corresponds to middle time of the season (Table 4).

Table 5. Data by determining rate of change of the brightness in individual seasons

Season	Middle date JD2400000+	φ_{min}	φ_{max}	dφ	dm	|dm/dφ|
1	45357	0.053	0.286	0.694	−0.33	0.48
2	46440	0.829	0.327	0.502	0.34	0.68
3	46738	0.289	0.961	0.672	0.2	0.30
4	47452	0.188	0.539	−0.351	0.24	0.68
5	47814	0.262	0.814	−0.552	0.35	0.63
6	48906	0.103	0.659	−0.555	0.25	0.45
7	49247	0.080	0.528	−0.447	0.2	0.45
8	52953	0.734	0.149	0.585	0.359	0.61
9	54806	0.418	0.891	−0.472	0.303	0.64
10	57896	0.318	0.973	−0.655	−0.268	0.41

On the data of Table 5 a graph of changes of magnitude |dm/dφ| for different seasons is built, which is given in Fig.8. As seen from Fig.8 the gradient of the stellar magnitude by phases changes approximately twice. Over range of time

about 12539 days, we found two waves of the parameter change | dm/dφ |. This testifies that, besides to the rapid day by day brightness changes, which are occurred with the existence of spots on the surface, possibly, there is an additional mechanism of variability with has more large characteristic time. The long time activity cycles in young stars may be related either by presence of an additional component in the system, or existing magnetic activity, alike the 11-year solar cycle.

In Fig.9 is shown a phase light curves for different seasons for three groups, given in Table 5. As seen from Fig.9, in groups designed as mas7 and mas10, the minimum and maximum of the light curve, differ insignificantly, whereas the group mas2 phases of the minimum and maximum, was shifted about 0.2P. Fig8.

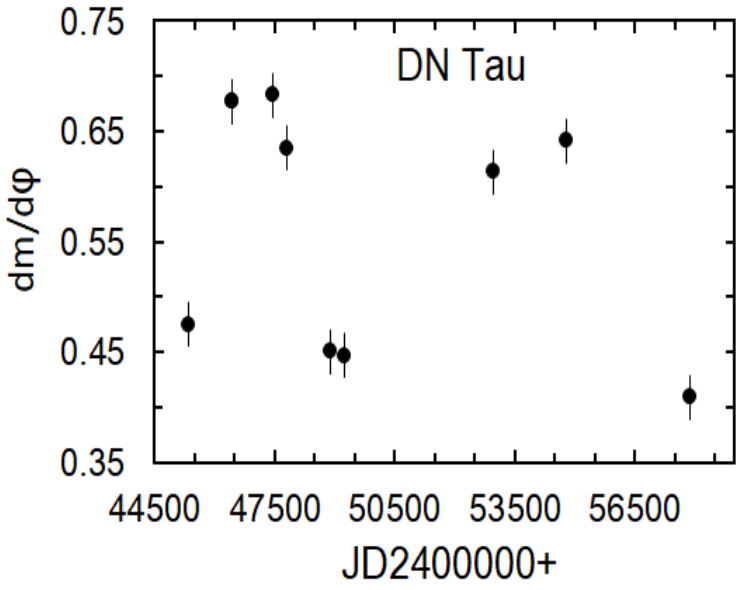

Fig. 8. The time variability of the star magnitude gradient dm/dφ, for different seasons.

Phase V - light curves for groups of mas2 (black dots), mas7 (circles) and mas10 (triangles) (see Table 3), where the groups numbers are corresponding to numbers, given in the first column of Table 5.

4. DISCUSSION AND CONCLUSIONS

So, in the work,the results of analysis of the master light curve and photometric specifications of the T Tauri type star DN Tau were given. It is shown, that besides seasonal changes of the star brightness, with maximum amplitude of

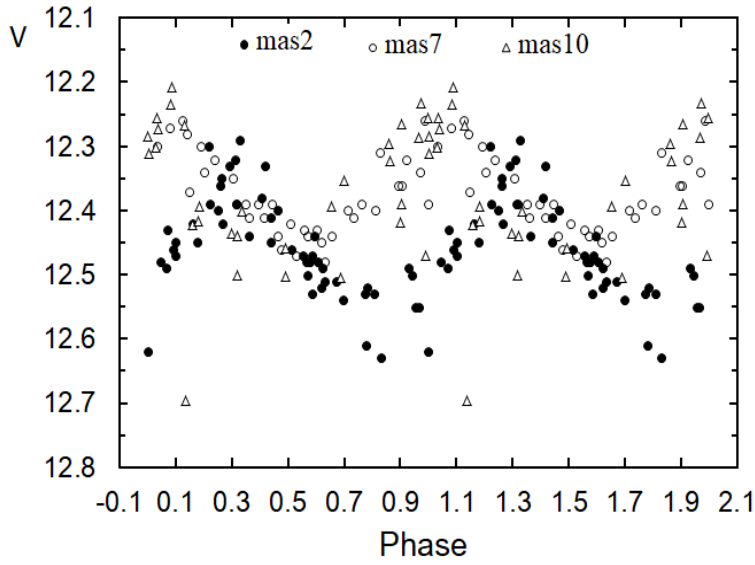

Fig. 9. Phase V - light curves for groups of mas2 (black dots), mas7 (circles) and mas10 (triangles) (see Table 3), where the groups numbers are corresponding to numbers, given in the first column of table 5.

0.5 mag to 1.0 mag, long time changes average annual values of brightness with a characteristic time of ten years are observed. Diagrams of distribution of the star brightness, carried out in different photometric bands, show that asymmetry is observed in the U and B bands, while, in the band V, distribution is symmetrical, and in the R and I bands, the brightness fluctuations are negligibly. It testifies about observation of flare activity of the star in the U and B bands, what can be explained by the presence of the accretion zone.

The analysis showed that the period of 6.3 days, previously determined by different methods,in separate seasons of observations is confidently stand out. However, the period values obtained in different years differ each from other by several tenth days. Such difference of the period values, apparently is not an error in period definition, but occurs as a result of real physical processes. Such a change, for example, could occur, when spots are migrated on the surface of the star by latitude, at differential rotation of the star's atmosphere, analogically to solar. On the obtained period values in different seasons, it is revealed that a period is changing at least for 0.3 days (see tab.2 and 3). In literature, various values of the rotation velocity $v \cdot sini$ of the star are given - from 12.3 km/s [23] to 8.1 km/s [24] (see Table 2), and on the latest data [13] by spectropolarimetric method was obtained 9 $\pm$ 1 km/s and for angle i = 35 $\pm$ 10°. If we assume,

that various values of the period are observed due to differential rotation in the atmosphere and migration of spots by latitude, then at angle of inclination o the axis 35° and in difference of periods by Δ P = 0.6 days upper limit for differences of rotation velocity relative to the equator would bee only 2 km/s.

It was shown, that phase light curve, for the period of 6.3 days show a significant shift by separate seasons. Maximum shift in phases is about 0.7P. The cause of such phase shifts can be occurred by appearing of star spots in different seasons, in various stellar longitudes.

We have obtained the following main conclusions: 1. It is shown that the seasonal changes in the brightness of the star in the V-band are 0.5 -1.0 mag. The annual average brightness values show a long-term cycle with a characteristic time of about 25 years. The variability of the brightness of the star, with various characteristic times is also observed, what indicated about existence of different mechanisms of brightness variation.

2. In the U and B bands, the brightness distribution has an asymmetrical form due to flare activity and in the R and I bands, the brightness distribution of the star in a large interval remains stable. It testifies that the contribution of the circumstellar disc of the star in change is insignificant and main variability mechanism is associated with the stellar surface.

3. An analysis of the star's light curve by different seasons allows to detecting clearly the 6-day period of brightness variability, defined previously by other authors. The distinction in the value of period for different seasons on a few tenths of days. For average value of the period by all seasons was obtained P = 6.231 $\pm$ 0.089 days.

4. It is shown that the value of period by different seasons may differ until 0.7 days. Besides, the phase shift of the maximum and minimum of seasonal phase light curves is discovered. It was put forward assumption, that the reason of change of period values 6.3 days in different seasons may be the differential rotation of photosphere and migration of spots by stellar latitude. The reason of phase shift of the seasonal light curves may be migration of spots along of the longitude.

5. It is shown that in seasonal phase light curves over a 6-day period, the rate of brightness change from maximum to minimum and vice versa is changing from season to season. Two limited values of brightness variation gradient by phase | dm/dφ | were obtained, about from 0.65 to 0.45. There is a long time cycle in variations of this parameter.

ACKNOWLEDGMENTS

This work was supported by the Science Development Foundation under the President of the Republic of Azerbaijan – Grant № EİF-BGM-4-RFTF-1/2017-21/07/1.

REFERENCES

1. Joy, A.H. Bright line stars among the Taurus dark clouds. 1949, ApJ, 110, 424

2. Herbig, G.H. Radial velocities and spectral types of T Tauri stars. 1977, ApJ, 214, 747

3. Cohen, M., Kuhi L.V. Observational studies of pre-main- sequence evolution. 1979, ApJS, 41, 743

4. Feigelson, E.D., Kriss, G.A. A search for weak H-alpha emission line pre-main-sequence stars. 1983, AJ, 88, 431

5. Rydgren, A.E., Strom, S.E., Strom, K.M. The nature of the objects of Joy - A study of the T Tauri phenomenon. 1976, ApJS, 30, 307

6. Petit, M. Contrib. Osserv. Astrof. Univ. Padova in Asiago, 1958, 95, 29.

7. Bouvier, J., Bertout, C., Bouchet, P. DN Tauri - A spotted T Tauri star. 1986, A&A, 158, 149

8. Vrba, F.J., Rydgren, A.E., Chugainov, P.F., et al. Further evidence for rotational modulation of the light from T Tauri stars. 1986, ApJ, 306, 199

9. Vrba, F.J., Chugainov, P.F., Weaver, Wm.B., Stauffer, J.S. Photometric and spectroscopic monitoring of AA Tau, DN Tau, UX Tau A, T Tau, RY Tau, LK CA 4, and LK CA 7. 1993, AJ, 106, 1608

10. Prato, L., Huerta, M., Johns-Krull, C.M. et al. A Young-Planet Search in Visible and Infrared Light: DN Tauri, V836 Tauri, and V827 Tauri. 2008, ApJ, 687, L103

11. Walter, F.M., Kuhi, L.V. The smothered coronae of T Tauri stars. 1981, ApJ, 250, 254

12. Walter, F.M., Kuhi, L.V. X-ray photometry and spectroscopy of T Tauri stars. ApJ, 1984, 284, 194

13. Donati, J.F., Gregory, S.G., Alencar, S.H.P. et al. Magnetospheric accretion on the fully convective classical T Tauri star DN Tau. 2013, MNRAS 436, 881

14. Percy, J.R., Gric, W.K., Wong, J.C.Y. Self-Correlation Analysis of the Photometric Variability of T Tauri Stars. 2006, PASP, 118, 1390

15. Bouvier, J., Cabrit, S., Fernandez, M., Martin, E.L., Matthews, J.M. Coyotes-I: the Photometric Variability and Rotational Evolution of T-Tauri Stars. 1993, A&A, 272, 176

16. Абдуллаев, Б.И., Алекберов, И.А., Гюльмалиев, Н.И., и др. Новый фотометр – поляриметр С ПЗС- камерой. 2012, ААЖ, , 8, №4, 39-49.

17. Herbst, W., Herbst, D.K., Grossman, E.J., et al. Catalogue of UBVRI photometry of T Tauri stars and analysis of the causes of their variability. 1994, AJ, 108, 1906 (http://wesfiles.wesleyan.edu/home/wherbst/web/TTauriDataBase/)

18. Grankin, K.N., Melnikov, S.Yu., Bouvier, J., et al. Results of the ROTOR-program I. The long-term photometric variability of classical T Tauri stars. 2007, A&A, 461, 183

19. http://www.astrouw.edu.pl/asas/

20. Scargle, J.D. Studies in astronomical time series analysis. Statistical aspects of spectral analysis of unevenly spaced data. 1982, ApJ, 263, 835

21. Horne, J.H., Balinas, S.L. A Prescription For Period Analysis Of Unevenly Sampled Time Series. 1986, ApJ, 302, 757

22. Antokhin, I., Bertrand, J.- F., Lamontagne, R., Moffat, A.F.J. The enigmatic WN8 stars: intensive photometry of four southern stars on time scales from 30 min to 3 months. 1995, AJ, 109, 817

23. Nguyen, D.C., Brandeker, A., van Kerkwijk, M.H., et al. Close companions to Young Stars. I. A Large Spectroscopic Survey in Chamaeleon I and Taurus-Auriga. 2012, ApJ, 745, 119

24. Appenzeller, I., Bertout, C., Stahl, O. Edge-on T Tauri stars. 2005, A&A, 434, 1005

25. Artemenko, S.A., Grankin, K.N.; Petrov, P.P. Rotation Effects in Classical T Tauri Stars. 2012, Astron.Lett., 38, 783

26. Bouvier, J., Bertout, C. Spots on T Tauri stars. 1989, A&A, 211, 99

27. Percy, J.R. Grynko, S., Seneviratne, R., Herbs

DN TAU ULDUZUNUN İŞIQ ƏYRİSİNİN TƏHLİLİ

N. Z. İsmayılov, S. Ə. Alışov, N. İ. Gülmalıyev

N.Tusi adına Şamaxı Astrofizika Rəsədxanası,
Azərbaycan Milli Elmlər Akademiyası, Şamaxı rayonu, Azərbaycan

Klassik T Buğa tipli DN Tau ulduzunun 2016-2017-ci illərdə ŞAR-da aparılmış BVR fotometrik müşahidələrinin nəticələri verilmişdir. Çoxillik işıq əyrisinin təhlili göstərmişdir ki, V-zolaqda mövsüm ərzində dəyişmələr 0.5m -1.0m aralığında baş verir. Parlaqlığın orta illik qiymətlərii 25 illik uzunmüddətli xarakterik vaxtla dəyişir. Parlaqlığın müxtəlif mövsümlər üzrə dəyişməsinin təhlili aydın şəkildə əvvəl digər müəlliflər tərəfindən təyin edilmiş 6-günlük periodun olduğunu aşkar etməyə imkan vermişdir. Periodun formal orta qiyməti müxtəlif mövsümlərə görə P = 6.231±0.089 gün alınmışdır. Göstərilmişdir ki, mövsümi işıq əyrilərində periodun qiyməti bir neçə onda bir sutka fərqlənir və periodun maksimum və minimum fazaları dəyişir. Güman olunur ki, fazaların müşahidə olunan sürüşmələri və 6-günlük periodun qiymətinin dəyişməsi ləkələrin miqrasiyası və ulduz atmosferinin differensial fırlanması nəticəsində baş verə bilər.

Açar sözlər: Ulduzlar: ulduzəmələgəlmə – Ulduzlar: baş-ardıcıllıq – Ulduzlar: – fərdi: – DN Tau ulduzu

THE INVESTIGATION OF THE INTERSTELLAR ENVIRONMENT IN THE DIRECTION OF THE κ CAS SUPERGIANT.

A. Kh. Rzaev [a*], ***V. V. Shimansky*** [b]

[a] *Special Astrophysical Observatory of the Russian Academy of Sciences, Nizhnij Arkhyz, Russia*

[b] *Kazan Federal University, Kazan, Russia*

The interstellar lines and diffuse bands in the spectrum of the supergiant κ Cas were investigated on the basis of CCD–echelle–spectra with high resolution. The synthetic spectrum with parametres T_{eff} = 21500, log g=2.45, $\upsilon \sin i$ = 83 km s^{-1}, ξ = 15 km s^{-1} was calculated for detection of bands against the background of the star spectrum. About 11 interstellar lines and 91 diffuse bands were identified. About 14 absorption details were additionally detected which could be the diffuse bands. The spectrophotometric parametres of interstellar lines and diffuse bands were defined with a good accuracy. Atlases of the ranges of the observable and calculated spectra were presented, where the interstellar diffuse bands are located.

Keywords: ISM: lines and bands – ISM: molecules – stars: individual – κ Cas

1. INTRODUCTION

The first diffuse interstellar bands (DIBs) were detected in the spectra obtained in the Lick observatory in 1922 [4] . Their interstellar origin have soon been established and tens others intensive DIBs were identified by the classical spectroscopy method. In the optical diapason of the spectrum, with the advent of the CCD echelle spectrographs, more than 400 weak DIBs have been detected and their central wave lengths were found [10]. It should be noted that up to now neither of them is confidently identified also the nature of them is unknown. To date, as possible carriers the DIB, are known some candidates (for the review see [6, 19]): polycyclic aromatic hydrocarbons (PAHs) [18]; C-chains [14]; fullerenes (C_{60^+}) [1]. They are trying to find a correlations between equivalent width of

* E-mail: abid@sao.ru

identified DIBs in different ranges of the spectrum for revealing of carriers and physical conditions their formation. The correlation testifies that various DIBs and molecular lines arise in the associated physical regions of the diffuse clouds [13]. Finally considerable quantity of weak DIBs can lead to convincing identifications of various absorbers the DIBs [10]. But only in single instances the atlases were drawn up and spectrophotometric parameters (W_λ, $R_0 = 1 - r_0$, FWHM) of the identified DIBs were defined with a good accuracy [3,9,10,12,20,24].

About 380 and 414 DIBs were accordingly identified in the spectra of the stars HD 204827 ($E_{B-V} = 1.11$) and HD 183143 ($E_{B-V} = 1.27$) in the spectral diapason λ3900–8100 Å [9,10]. The central wave lengths, FWHM and equivalent width for all DIBs were defined. It is noticed that both an abundances of the big molecules forming the DIBs and physical conditions in clouds located in the line of these two stars considerably differ [10]. All it testifies that similar investigations need to carry out for many stars with different degree of reddening. In this study the interstellar lines (ISL) and DIBs were investigated in the spectrum of the κ Cas B0.7 Ia supergiant (with moderate degree of the reddening E(B-V) = 0.33 [21]) on the basis of CCD-echelle spectra with the high spectral resolution and the signal-to-noise relation S/N.

2. OBSERVATIONAL DATA AND THEIR REDUCTION

Spectroscopic observations were carried out with the 2-m Ritchey-Chretien-Coude telescope at Peak Terskol Observatory during 11 nights from August 31 to October 7, 1999. In fours spectra were obtained within 3 nights, and in other nights – in twos ones which were averaged for every night. The spectra had 87 orders, registered wavelength region λ3550–10100 Å and spectral resolution about $\lambda/\Delta\lambda = 45000$ [17].

DIBs have been discovered in the wave length diapason about λ4750–7000 Å. In the extremal ranges of this diapason the S/N relation is about $400 \leq S/N \leq 450$ in the separate spectrum. The maximum value of this relation is in spectrum range λ5650 Å and is about $500 \leq S/N \leq 600$. In the total spectrum the value is in the limits $700 \leq S/N \leq 1300$. In separate spectra in the ranges where there are the interstellar lines CaI λ4226, CH^+ λ4232, CH λ4300, KI λ7698 and CaII λ3933 the relation accordingly are $250 \leq S/N \leq 300$ and $180 \leq S/N \leq 250$.

We reduced the echelle spectrum by the standard method using DECH95[1)] software package. We measured the spectrophotometric parameter (W_λ, r_0) and radial velocity of the lines using the DECH20t[1] software package. For wavelength

[1)] http://www.gazinur.com

calibration in separate nights the spectra of the Sky, Moon and Procyon were obtained. We used H_2O and O_2 telluric lines to set the zero point of the radial-velocity scale. The rms error from the average for 60 telluric lines are not exceed $|0.1|\pm0.1\,\mathrm{km\,s^{-1}}$.

3. THE SPECTROPHOTOMETRIC PARAMETERS AND RADIAL VELOCITIES OF THE IDENTIFIED LINES

If we compare ISLs and DIBs in coordinates $r(\lambda)$ then we will observe displacement between profiles of the identical lines. This is due to the fact that their radial velocities do not change with time but the heliocentric correction of the radial velocity differs for different dates of the observations. The correction value ΔV (i.e. $\Delta\lambda$) varies based on wave lengths for different region of the spectrum (i.e. for different ISLs and DIBs). When summing spectra these corrections have been taken into account both for different regions of the spectrum and for different dates of the observations. For reliability the radial velocities and spectrophotometric parameters of the ISLs and DIBs were defined for each spectrum separately and not over the total ones. Further the average value and root-mean-square deviation from this average has been defined for each parametre of line.

The radial velocity measurement of the ISLs was realized at half level of the line intensity (FWHM) and the line core. In the previous case the obtained values of the radial velocity for different lines (and for different dates) well coincided among themselves. The RMS deviation from the average was also much less than in the second case. Therefore the radial velocities of the identified DIBs were also measured at FWHM level.

In the spectrum κ Cas the interstellar lines CaI λ 4226, CaII (K), NaI (D_2, D_1), KI λ 7699, CH^+ λ 4232 and CH λ 4300 have been investigated with the ultrahigh resolution [2, 7, 8, 22, 23]. At least well divided three components are observed at these lines. But in our case ($\lambda/\Delta\lambda = 45000$) these components merge together and demonstrate identical values of the radial velocity about -17.0 ± 0.5, -17.2 ± 1.5, -17.1 ± 0.9, -16.6 ± 0.8, -16.5 ± 0.4, $-16.9\pm0.9\,\mathrm{km\ s^{-1}}$ accordingly for CaII λ 3933, CaI λ 4226, CH^+ λ 4232, CH λ 4300, NaI(D_2, D_1) and KI λ 7699 (Table 1). Influence of the separate components on positional and spectrophotometric parameters of the line is not observed within measurements errors. In our case 11 interstellar lines was detected in the spectrum κ Cas. The radial velocities, W_λ, $FWHM$, $R_0 = 1 - r_0$ of nine interstellar lines (without CaI λ 3968, KI λ 7664) and accuracy of their definition are listed in the Table 1.

The synthetic spectrum with parametres T_{eff} = 21500, log g=2.45, $v\sin i$ = 83 $\mathrm{km\,s^{-1}}$, ξ = 15 $\mathrm{km\,s^{-1}}$ was calculated for the detection of the

Table 1: Heliocentric radial velocities and spectrophotometric parametres of interstellar lines in the spectrum κ Cas

Element	λ_c Å	W_λ mÅ	FWHM Å	R_0 1-r_0	V kms^{-1}
CaII	3933.66	261.1 ± 4.2	0.324 ± 0.005	0.803 ± 0.006	-17.0 ± 0.5
CH^+	3957.71	10.6 ± 1.1	0.28 ± 0.03	0.036 ± 0.005	-17.1 ± 1.1
CaI	4226.73	7.8 ± 1.5	0.29 ± 0.03	0.029 ± 0.005	-17.2 ± 1.5
CH^+	4232.54	13.0 ± 1.6	0.31 ± 0.04	0.041 ± 0.003	-17.1 ± 0.9
CO^+	4250.40	3.6 ± 0.5	0.24 ± 0.04	0.015 ± 0.003	-17.1 ± 1.7
CH	4300.32	9.9 ± 1.5	0.26 ± 0.03	0.041 ± 0.002	-16.6 ± 0.8
NaI	5889.95	527.4 ± 2.6	0.523 ± 0.006	0.837 ± 0.006	-16.5 ± 0.4
NaI	5895.93	498.2 ± 2.3	0.505 ± 0.007	0.712 ± 0.004	-16.5 ± 0.4
KI	7698.97	88.0 ± 2.1	0.52 ± 0.02	0.167 ± 0.008	-16.9 ± 0.9

bands against the background of the star spectrum. The computation spectrum well describes the observable stellar ones. The DIBs identification was carried out under the lists taken from studies [3, 9, 10, 12, 20, 24]. Strongly blended DIBs (polluted) by stellar or telluric lines have not been examined by us.

Up to now the finding of the central wave length for identified DIBs remains a challenging issue. In studies [3, 9, 10, 12, 20, 24] where similar identifications were carried out, the difference between values of the central wave length reaches up to 0.24 Å even in case of well-known DIBs λ 5780, 5797 (see Table 2 in [10]).

One can see from Table 1 in our case the values of the radial velocity of all interstellar lines are in the interval $-17.2 \leq V \leq -16.5$. We have assumed that the radial velocities of the all identified DIBs should also be in this diapason. Defined thus the radial velocities and corresponding central wave lengths of the DIBs are listed in Table 2. If the wave length to within ± 0.04 Å (i.e. does not exceed the error of the radial velocity measurement for weak DIBs) coincides with that of above listed six studies then the superscript indicate the reference to this work (Table 2, the first column). The index "o" is meant – our definition and the wave length found by us differs from other works more than on ± 0.04 Å. Fig. 1 is shown the atlases of the ranges where the DIBs in the kCas spectrum were identified.

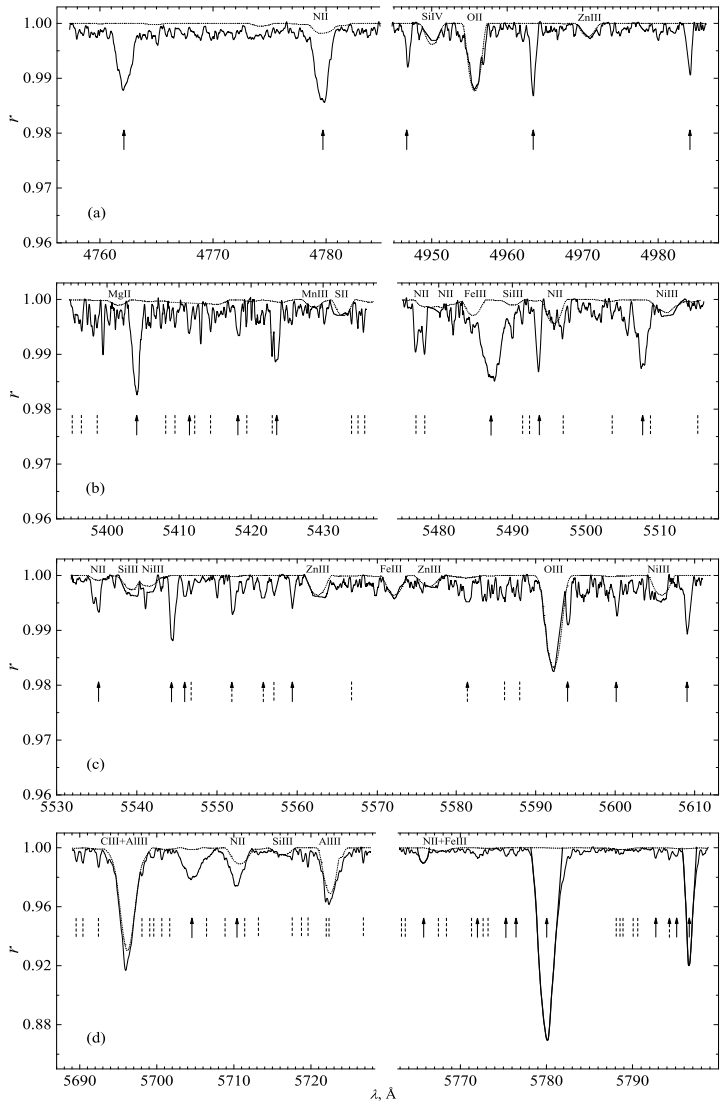

Fig. 1: The atlas of the spectral ranges of the spectrum κ Cas where are observed diffuse interstellar bands. The dashed line – calculation spectrum. The elements of the stellar lines are pointed. Vertical continuous and dotted arrows relative point to the positions of the identified and assumed bands, vertical dashed lines –telluric lines.

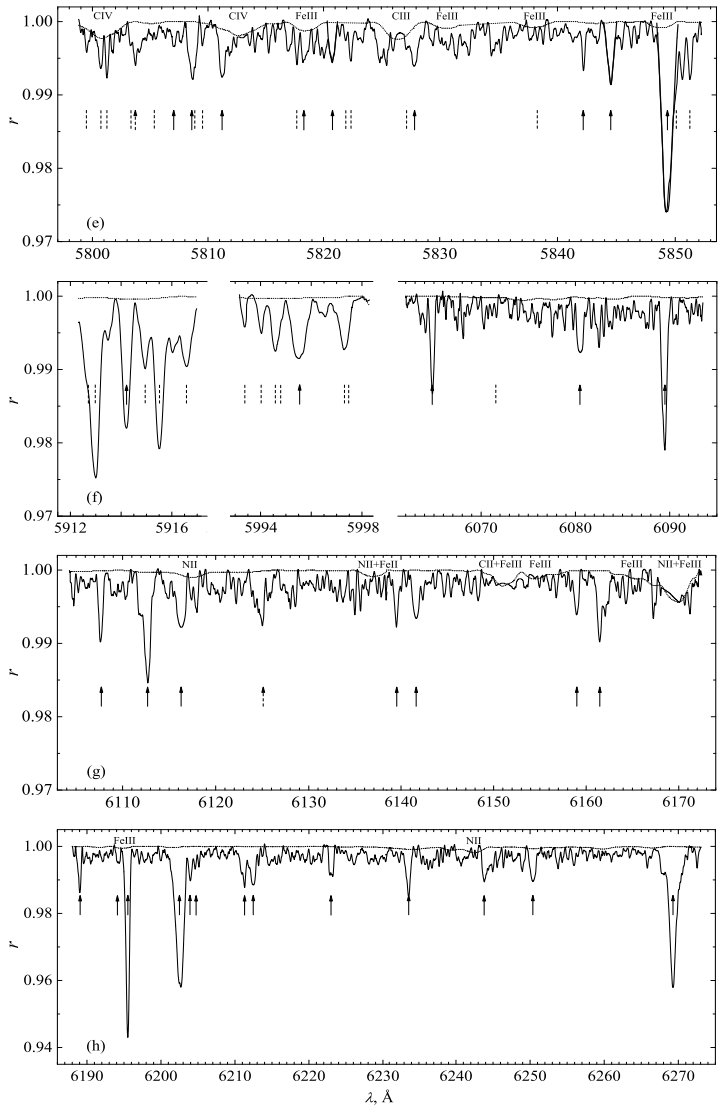

Fig. 1 (continued)

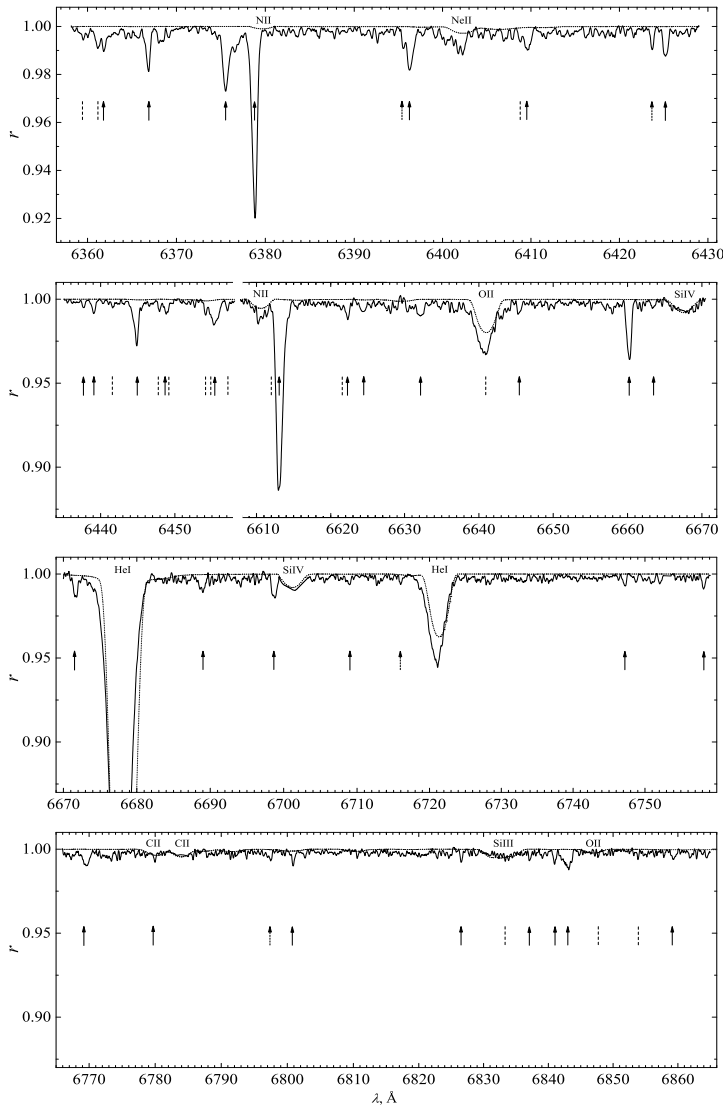

Fig. 1 (continued)

The software package DECH20t allows one to define equivalent width in the various ways. If the line profile is complex it is possible to apply the method which allows to construct the line profile manually. The examples of the manually constructed profiles are shown in Fig. 1 (d, e) by bold lines. The spectrophotometric parametres and their measurement errors of the identified DIBs are presented in the 2–4 columns of the Table 2. It should be noted that influence of the instrumental profile is slightly. In blue range of the spectrum where weak interstellar lines CaI, CO^+, CH are observed the FWHM value of the instrumental profile does not exceed 0.09, and in red range - 0.14 Å.

4. RESULTS AND DISCUSSION

In the spectrum κ Cas in the range λ 4750 - 6870 Å about 91 DIBs were identified by us. Their equivalent width, FWHM, the central depths and radial velocities are defined. In the case of the strongest DIBs λ5780, 6613 and 5797 the equivalent width were defined to within 4%. For 11 and 19 DIBs that have the equivalent width accordingly are in the interval of $20.0 \leq W_\lambda \leq 70.0$, and $9.0 \leq W_\lambda \leq 18.0$ mÅ accuracy of definition are ≤ 10 and 14.0 ± 2.0 %. For others weak DIBs ($2.0 \leq W_\lambda < 9.0$ mÅ) accuracy of definition is 20.0 ± 2 %.

In the spectrum κ Cas the DIBs λ5780, 5797 and 5849 were investigated (W_λ are defined) in the study [5, 13], the radicals CH^+ λ4232 and CH λ4300 – [2, 11, 13], the interstellar line KI λ6799 and the DIBλ6613 – [21]. Comparison of the data from the above mentioned studies with our data is shown that if the parametres were defined on the basis of spectra with $\lambda/\Delta\lambda \geq 40000$, $S/N > 100$ the difference of the values does not exceed 8%.

In [16] in spectra κ Cas ($\lambda/\Delta\lambda$ = 60000, S/N≥500) six DIBs λ5780, 5797, 5830, 6196, 6379, 6614 were investigated and the central depths were defined. Coincidence of these values with ours very good. The difference of the values does not exceed 2%. All it testifies good accuracy of our measurements.

The radial velocities of the interstellar lines and DIBs were measured at the level FWHM of their profiles. The measurements have shown that in this case the average value of the radial velocity for all interstellar lines (within of the measurement errors) is obtained identical, and a root-mean-square deviation from an average is minimum. Our measurements have shown that the radial velocities of the interstellar lines are in the interval $-17.2 \leq V \leq -16.5$ km s^{-1} (Table 1). The radial velocities of all the studied DIBs were measured by this principle and their central wave lengths were defined. Thus the found values of the central wave lengths are in good agreement with ones from other studies. For 33, 18, 8, 4, 2 and 4 DIBs these values correspondingly (with accuracy ±0.04 mÅ) coincide with the data from study [3,9,10,12,20,24]. In Table 2 these references are noted with

Table 2: Heliocentric radial velocities and spectrophotometric parameters of diffuse interstellar bands in the spectrumκ Cas. Indexes *a, b, c, d, e, f* accordingly point to the studies [3,9,10,12,20,24], *o* - our definitions.

λ_c Å	W_λ mÅ	$FWHM$ Å	R_0 $1-r_0$	V $km\,s^{-1}$
4762.62^a	17.8 ± 2.5	1.51 ± 0.05	0.014 ± 0.002	-16.7 ± 1.5
4780.04^c	19.6 ± 2.1	1.34 ± 0.04	0.015 ± 0.002	-16.8 ± 1.4
4947.38^b	5.1 ± 0.9	0.57 ± 0.03	0.008 ± 0.001	-16.9 ± 1.7
4963.90^c	9.8 ± 1.5	0.71 ± 0.02	0.013 ± 0.002	-16.5 ± 1.7
4984.73^d	7.0 ± 1.4	0.62 ± 0.02	0.010 ± 0.001	-17.2 ± 1.8
5404.56^b	21.3 ± 1.8	1.13 ± 0.03	0.018 ± 0.002	-17.0 ± 1.1
5418.87^b	4.9 ± 1.0	0.74 ± 0.03	0.007 ± 0.001	-17.1 ± 2.1
5424.10^b	9.5 ± 1.3	0.84 ± 0.03	0.012 ± 0.001	-17.0 ± 2.0
5487.70^a	42.1 ± 4.3	2.97 ± 0.07	0.015 ± 0.002	-17.1 ± 1.6
5494.10^c	9.4 ± 1.2	0.72 ± 0.03	0.013 ± 0.002	-16.5 ± 1.8
5508.35^c	16.1 ± 2.5	1.34 ± 0.06	0.012 ± 0.002	-17.1 ± 1.5
5535.20^b	3.1 ± 0.6	0.59 ± 0.05	0.006 ± 0.001	-17.2 ± 1.9
5544.96^c	8.5 ± 1.3	0.67 ± 0.02	0.013 ± 0.001	-17.0 ± 1.2
5546.48^a	2.6 ± 0.5	0.65 ± 0.03	0.005 ± 0.001	-17.1 ± 1.3
5560.03^b	2.7 ± 0.5	0.51 ± 0.03	0.007 ± 0.001	-16.8 ± 1.1
5594.60^b	5.9 ± 1.2	0.67 ± 0.03	0.010 ± 0.002	-16.9 ± 1.7
5600.76^o	5.1 ± 1.0	0.62 ± 0.04	0.008 ± 0.001	-17.2 ± 1.8
5609.73^c	8.2 ± 1.6	0.74 ± 0.06	0.011 ± 0.002	-16.7 ± 1.2
5705.08^b	49.2 ± 4.6	2.45 ± 0.25	0.021 ± 0.001	-17.0 ± 2.0
5766.25^a	10.2 ± 1.4	1.07 ± 0.07	0.010 ± 0.002	-17.0 ± 1.2
5772.61^b	4.0 ± 0.8	0.58 ± 0.05	0.008 ± 0.001	-17.0 ± 1.2
5775.90^b	3.7 ± 0.8	0.59 ± 0.05	0.007 ± 0.001	-17.1 ± 0.9
5780.55^f	268.6 ± 8.7	2.00 ± 0.05	0.132 ± 0.003	-16.7 ± 0.8
5793.21^b	3.1 ± 0.7	0.35 ± 0.06	0.008 ± 0.001	-16.8 ± 1.8
5795.62^o	3.4 ± 0.7	0.60 ± 0.09	0.006 ± 0.001	-16.8 ± 2.1
5797.16^o	70.8 ± 2.8	0.86 ± 0.03	0.081 ± 0.003	-16.8 ± 0.8
5809.22^b	5.6 ± 0.9	1.07 ± 0.06	0.008 ± 0.001	-17.2 ± 2.1
5811.79^o	5.3 ± 1.0	0.61 ± 0.04	0.008 ± 0.001	-17.0 ± 2.0
5821.28^o	3.2 ± 0.7	0.59 ± 0.05	0.006 ± 0.001	-16.8 ± 1.5
5828.40^d	4.4 ± 0.9	0.71 ± 0.06	0.006 ± 0.001	-16.8 ± 1.6
5842.76^o	2.6 ± 0.6	0.35 ± 0.02	0.007 ± 0.001	-17.0 ± 0.8
5844.96^a	5.1 ± 1.0	0.57 ± 0.03	0.009 ± 0.001	-16.7 ± 1.1
5849.88^a	26.4 ± 2.2	1.01 ± 0.06	0.026 ± 0.002	-16.8 ± 0.8
5914.79^b	6.6 ± 1.2	0.36 ± 0.03	0.018 ± 0.001	-17.1 ± 1.0
5996.08^o	5.5 ± 1.1	0.62 ± 0.04	0.010 ± 0.001	-17.1 ± 1.3

Table 2 (continued)

λ_c Å	W_λ mÅ	FWHM Å	R_0 1-r_0	V $km\,s^{-1}$
6065.36^d	6.1 ± 1.2	0.47 ± 0.02	0.013 ± 0.001	-16.8 ± 0.9
6081.10^a	5.9 ± 1.1	0.78 ± 0.05	0.008 ± 0.001	-17.2 ± 1.5
6089.99^o	12.6 ± 1.2	0.61 ± 0.04	0.021 ± 0.001	-16.9 ± 1.1
6108.18^a	5.2 ± 1.0	0.55 ± 0.05	0.010 ± 0.001	-16.6 ± 1.4
6113.29^a	11.8 ± 1.8	0.77 ± 0.06	0.017 ± 0.002	-17.1 ± 1.0
6116.84^a	7.9 ± 1.5	1.09 ± 0.07	0.008 ± 0.001	-16.6 ± 1.2
6140.04^a	4.1 ± 0.9	0.50 ± 0.05	0.009 ± 0.001	-16.9 ± 1.6
6142.20^a	5.3 ± 1.1	0.82 ± 0.03	0.007 ± 0.001	-17.2 ± 2.1
6159.52^o	3.4 ± 0.6	0.59 ± 0.03	0.006 ± 0.001	-17.0 ± 1.5
6161.98^a	6.3 ± 1.2	0.55 ± 0.04	0.011 ± 0.002	-16.5 ± 2.0
6189.55^a	5.4 ± 1.1	0.38 ± 0.04	0.014 ± 0.001	-16.7 ± 1.2
6194.73^c	1.9 ± 0.4	0.41 ± 0.06	0.006 ± 0.001	-17.1 ± 2.1
6196.09^a	31.4 ± 1.4	0.54 ± 0.02	0.058 ± 0.002	-17.2 ± 1.1
6203.14^a	50.1 ± 4.7	1.17 ± 0.07	0.044 ± 0.002	-17.0 ± 1.5
6204.54^o	5.3 ± 1.0	0.59 ± 0.04	0.010 ± 0.001	-17.0 ± 2.1
6205.20^a	2.7 ± 0.5	0.36 ± 0.05	0.008 ± 0.001	-16.9 ± 1.8
6211.80^a	5.7 ± 1.0	0.51 ± 0.04	0.013 ± 0.002	-16.7 ± 1.6
6213.00^a	8.7 ± 1.4	0.79 ± 0.03	0.011 ± 0.001	-16.7 ± 1.3
6223.61^e	6.1 ± 1.1	0.69 ± 0.05	0.010 ± 0.001	-17.2 ± 1.6
6234.11^a	10.7 ± 1.3	0.71 ± 0.04	0.015 ± 0.001	-16.5 ± 1.1
6244.46^b	6.8 ± 1.3	0.67 ± 0.05	0.011 ± 0.001	-16.7 ± 2.1
6250.97^b	9.1 ± 1.1	0.89 ± 0.07	0.011 ± 0.001	-16.9 ± 1.7
6269.85^a	42.8 ± 4.1	1.02 ± 0.05	0.042 ± 0.002	-16.8 ± 1.5
6362.44^a	5.6 ± 1.1	0.51 ± 0.03	0.011 ± 0.001	-16.6 ± 1.8
6367.41^e	11.8 ± 1.8	0.52 ± 0.05	0.022 ± 0.002	-16.8 ± 1.4
6376.15^o	21.1 ± 2.3	0.79 ± 0.04	0.027 ± 0.001	-16.9 ± 1.2
6379.39^o	54.3 ± 1.1	0.67 ± 0.02	0.080 ± 0.002	-17.0 ± 0.8
6396.97^f	14.9 ± 2.3	0.81 ± 0.03	0.018 ± 0.001	-17.0 ± 1.5
6410.20^b	8.4 ± 1.3	0.79 ± 0.05	0.010 ± 0.001	-16.8 ± 2.0
6425.78^a	8.3 ± 1.5	0.65 ± 0.06	0.012 ± 0.002	-16.9 ± 1.7
6438.28^a	2.4 ± 0.5	0.43 ± 0.02	0.006 ± 0.001	-16.8 ± 2.1
6439.68^o	4.6 ± 0.9	0.51 ± 0.03	0.010 ± 0.002	-17.0 ± 2.1
6445.41^a	14.4 ± 2.1	0.53 ± 0.02	0.028 ± 0.002	-16.9 ± 1.8
6449.44^o	5.1 ± 1.0	0.49 ± 0.02	0.011 ± 0.001	-17.1 ± 2.1
6456.02^a	15.2 ± 2.1	0.87 ± 0.09	0.016 ± 0.001	-16.9 ± 1.8
6520.85^o	17.1 ± 2.5	1.05 ± 0.05	0.017 ± 0.003	-16.7 ± 1.9
6613.72^d	120.6 ± 5.4	0.99 ± 0.02	0.114 ± 0.002	-17.2 ± 0.8

Table 2 (continued)

λ_c Å	W_λ mÅ	$FWHM$ Å	R_0 $1-r_0$	V $km\,s^{-1}$
6622.92^o	6.4 ± 1.2	0.55 ± 0.05	0.013 ± 0.002	-17.0 ± 1.2
6624.93^a	7.2 ± 1.3	1.05 ± 0.05	0.008 ± 0.002	-16.8 ± 2.0
6632.76^o	11.0 ± 1.9	1.13 ± 0.03	0.010 ± 0.001	-16.9 ± 1.1
6646.05^a	5.8 ± 1.1	0.67 ± 0.04	0.010 ± 0.001	-17.0 ± 1.2
6660.82^a	26.8 ± 2.8	0.75 ± 0.05	0.036 ± 0.001	-17.0 ± 1.1
6664.05^a	3.7 ± 0.7	0.71 ± 0.07	0.007 ± 0.001	-16.9 ± 2.0
6672.27^b	9.4 ± 1.5	0.68 ± 0.05	0.014 ± 0.002	-16.7 ± 1.9
6689.51^o	10.5 ± 1.6	0.94 ± 0.07	0.011 ± 0.001	-17.0 ± 2.1
6699.36^a	12.1 ± 1.9	0.86 ± 0.06	0.014 ± 0.002	-16.8 ± 1.8
6709.58^o	3.2 ± 0.6	0.51 ± 0.04	0.007 ± 0.001	-17.0 ± 2.1
6747.80^e	3.6 ± 0.8	0.49 ± 0.03	0.008 ± 0.001	-16.8 ± 2.0
6758.82^o	4.4 ± 0.9	0.51 ± 0.03	0.010 ± 0.001	-17.1 ± 2.1
6770.21^b	10.7 ± 1.6	1.08 ± 0.06	0.011 ± 0.001	-17.0 ± 1.7
6780.59^o	3.8 ± 0.7	0.50 ± 0.05	0.009 ± 0.002	-17.2 ± 1.9
6801.54^a	4.3 ± 0.8	0.46 ± 0.04	0.010 ± 0.001	-17.0 ± 1.8
6827.22^e	3.2 ± 0.6	0.42 ± 0.04	0.008 ± 0.001	-17.2 ± 2.0
6841.66^a	4.7 ± 0.9	0.53 ± 0.05	0.010 ± 0.001	-17.2 ± 1.8
6843.64^a	15.2 ± 3.9	1.38 ± 0.03	0.013 ± 0.002	-17.0 ± 2.1
6860.02^c	4.9 ± 0.9	0.94 ± 0.04	0.006 ± 0.001	-17.0 ± 2.3
may be DIBs				
5411.95	3.9 ± 0.7	0.60 ± 0.03	0.006 ± 0.001	-17.0 ± 1.9
5552.58	4.3 ± 0.6	0.64 ± 0.04	0.007 ± 0.002	-17.2 ± 1.6
5556.27	3.7 ± 0.9	0.92 ± 0.06	0.005 ± 0.001	-16.9 ± 2.1
5581.98	4.9 ± 0.9	1.02 ± 0.04	0.006 ± 0.001	-16.6 ± 1.8
5777.01	3.1 ± 0.5	0.49 ± 0.05	0.006 ± 0.001	-17.1 ± 1.2
5794.86	3.4 ± 0.8	0.39 ± 0.03	0.009 ± 0.001	-17.1 ± 1.9
5804.25	3.2 ± 0.7	0.49 ± 0.04	0.008 ± 0.002	-16.9 ± 2.1
6125.58	3.5 ± 0.9	0.43 ± 0.05	0.008 ± 0.001	-16.9 ± 2.1
6273.12	2.3 ± 0.5	0.29 ± 0.02	0.007 ± 0.001	-16.9 ± 1.2
6396.19	4.0 ± 0.8	0.44 ± 0.03	0.011 ± 0.001	-17.1 ± 2.1
6424.31	4.1 ± 0.6	0.42 ± 0.04	0.010 ± 0.001	-17.0 ± 1.7
6716.61	2.6 ± 0.6	0.46 ± 0.05	0.007 ± 0.001	-16.9 ± 1.8
6798.12	3.4 ± 0.7	0.52 ± 0.03	0.007 ± 0.001	-17.0 ± 2.0
6837.81	3.2 ± 0.6	0.45 ± 0.04	0.008 ± 0.001	-17.2 ± 2.1

corresponding indexes. For 22 DIBs the values of the central wave lengths defined by us do not coincide with other authors.

In addition 14 absorption details are also identified by us which may be diffuse bands. They are presented in the bottom part of Table 2. These details are present on all spectra, and are not stellar and telluric lines. For them the found average values of the spectrophotometric parametres and also rms deviation from them are in reasonable limits. We have also defined their central wave lengths by measuring the radial velocities by above mentioned principle (Table 2). In Fig. 1 these absorption details are noted by dotted vertical arrows.

REFERENCES

1. Campbell, E.K., Holz, M., Gerlich, D., Maier, J.P. Laboratory confirmation of C60(+) as the carrier of two diffuse interstellar bands. 2015, Nature, 523, 322

2. Federman, S.R. Measurements of CH and CH/+/ in diffuse interstellar clouds. 1982, ApJ, 257, 125

3. Galazutdinov, G.A., Musaev, F.A., Krelowski, J., Walker, J. Narrow Diffuse Interstellar Bands: A Survey with Precise Wavelengths. 2000, PASP, 112, 648 [DOI: 10.1086/316570]

4. Heger, M.L. The spectra of certain class B stars in the regions 5630A-6680A and 3280A-3380A. 1922, Lick Obs. Bull., 10, 337, 146

5. Herbig G.H., 1993, ApJ 407, 142

6. Herbig G.H., 1995, Annu. Rev. Astron. Astroph., **33**, 19

7. Hobbs, L.M. Observations of Interstellar CA i Lines. 1971, ApJ, 170, L85

8. Hobbs, L.M. Observations of interstellar lines of NA I and/or CA II toward 47 stars. 1978, ApJS, 38, 129

9. Hobbs, L.M., York, D.G., Snow, T.P., et. al. A Catalog of Diffuse Interstellar Bands in the Spectrum of HD 204827. 2008, ApJ, 680, 1256 [DOI: 10.1086/587930]

10. Hobbs, L.M., York, D.G., Thorburn J.A., et. al. STUDIES OF THE DIFFUSE INTERSTELLAR BANDS. III. HD 183143. 2009, ApJ, 705, 32

11. Jenniskens, P., Ehrenfreund, P., Desert, F.-X. Far UV nonlinear rise extinction in relation to CH and CH(+) abundances. 1992, A&A, 265, L1

12. Jenniskens, P. and Desert, F.-X. A survey of diffuse interstellar bands (3800-8680 A). 1994, A&AS, 106, 39

13. Krelowski, J., Ehrenfreund, P., Foing, B.H., et. al. On the relation between diffuse interstellar bands and simple molecular species. 1999, A&A, 347, 235

14. McCall, B.J., York, D.G., Oka, T. Observations of Diffuse Interstellar Bands Attributed to C-7. 2000, ApJ, 531, 329 [DOI: 10.1086/308453]

15. Merrill, P.W. Unidentified Interstellar Lines. 1934, PASP, 46, 206 [DOI: 10.1086/124460]

16. Moutou, C., Krelowski, J., d'Hendecourt, L., Jamroszczak, J. On correlations between diffuse interstellar bands. 1999, A&A, 351, 680

17. Musaev, F.A., Galazutdinov, G.A., Sergeev, A.V. et. al. The Coude-Echelle Spectrometer for the 2-meter Telescope at Peak Terskol. 1999, Kinematics Phys. Celest. Bodies, 15, 3, 216

18. Salama, F., Bakes, E.L.O., Allamandola, L.J., Tielens A.G.G.M. Assessment of the Polycyclic Aromatic Hydrocarbon–Diffuse Interstellar Band Proposal. 1996, ApJ, 458, 621

19. Snow, T.P., In: From Stardust to Planetesimals., Y.J. Pendleton, A.G.G.M. Tielens (eds.), ASP Conf. Ser. 122, Astronomical Society of the Pacific, San Francisco, 1997, 147.

20. Tuairisg, S.O., Cami, J., Foing, B.H., Sonnentrucker P., Ehrenfreund, P. A deep echelle survey and new analysis of diffuse interstellar bands. 2000, A&AS, 142, 225 [DOI: 10.1051/aas:2000148]

21. Wallerstein, G., Sandstrom, K., Gredel, R. A Preliminary Investigation of the Diffuse Interstellar Line at 8621 Å. 2007, PASP, 119, 1268

22. Welty, D.E., Hobbs, L. M. A High-Resolution Survey of Interstellar K I Absorption. 2001, ApJS, 133, 345

23. Welty, D.E., Hobbs, L.M., Morton, D.C. VizieR Online Data Catalog: Interstellar Ca I absorption. 2003, ApJS, 147, 61

24. Weselak, T., Schmidt, M., Krelowski, J. A new survey of diffuse interstellar bands (5650 - 6865 Å). 2000, A&AS, 142, 239

κ CAS ULDUZU İSTİQAMƏTİNDƏ ULDUZLARARASI MÜHİTİN ÖYRƏNİLMƏSİ

***A. X. Rzayev*[a], *V. V. Shimanski*[b]**

[a] *Xüsusi Astrofizika Rəsədxanası, Rusiya Elmlər Akademiyası, Nijniy Arxız, Rusiya*

[b] *Kazan Federal Universiteti, Kazan, Rusiya*

Yüksək spektral ayırdetmə güclü CCD–eşelle–spektrlər əsasında κ Cas ifratnəhəng ulduzunun spektrində ulduzlararası xətlər və diffuz zolaqlar tədqiq olunmuşdur. Ulduzun spektri fonunda diffuz zolaqlarını ayırd etmək üçün T_{eff} = 21500, log g=2.45, $\upsilon \sin i$ = 83 km s^{-1}, ξ = 15 km s^{-1} parametrləri əsasında nəzəri–sintetik spektr hesablanmışdır. 11 ulduzlararası xət və 91 diffuz zolağı aşkar edilmişdir. Əlavə 14 absorbsiya detalları aşkar olunmuşdur, ki bunları da diffuz zolaqlarına aid etmək olar. Ulduzlararası xətlər və diffuz zolaqlarının spektrofotometrik parametrləri yüksək dəqiqliklə təyin olunmuşdur. Ulduzlararası xətlərin və diffuz zolaqlarının spektrdə qeydə alınan oblastlarının həm nəzəri–sintetik, həm də müşahidə spektrinin atlasları tərtib edilib.

Açar sözlər: Ulduzlararası mühit: xətlər və zolaqlar – Ulduzlararası mühit: molekullar, ulduzlar: fərdi: κ Cas ulduzu